Technical Report Documentation Page

1. Report No.	2. Government Accession No.	3. Recipient's Catalog No.
SWUTC/14/600451-00010-1		

4. Title and Subtitle	5. Report Date
ENHANCED ADAPTIVE SIGNAL CONTROL USING DEDICATED SHORT-RANGE COMMUNICATIONS	May 2014
	6. Performing Organization Code

7. Author(s)	8. Performing Organization Report No.
Yunlong Zhang and Kamonthep Tiaprasert	Report 600451-00010-1

9. Performing Organization Name and Address	10. Work Unit No. (TRAIS)
Texas A&M Transportation Institute College Station, Texas 77843-3135	11. Contract or Grant No. DTRT12-G-UTC06

12. Sponsoring Agency Name and Address	13. Type of Report and Period Covered
Southwest Region University Transportation Center Texas A&M Transportation Institute College Station, Texas 77843-3135	Technical Report
	14. Sponsoring Agency Code

15. Supplementary Notes

Supported by a grant from the U.S. Department of Transportation University Transportation Centers Program and general revenues from the State of Texas.

16. Abstract

Connected vehicle technology with dedicated short-range communications can provide traffic information in a spatial domain that conventional fixed-point detectors cannot provide. However, because of low market penetration with this new data source, new measures to obtain other traffic parameters and new methodologies to use these new data for better signal control are needed. Arterial roads with multiple intersections and coordinate systems can benefit from these spatial domain data as it allows vehicles to move without being stopped.

For a heterogeneous traffic flow, multi-class cell transmission (M-CTM) is used to optimize signal timing control. M-CTM should work well in modeling traffic flow with signal coordination along an arterial where the platoon dispersion effect is significant and has to be accounted for in order to achieve accurate modeling results. Furthermore, queue length estimation was developed to use connected vehicle data without relying on a conventional detector. Lastly, an adaptive signal control based on the queue length estimation and connected vehicle technology was developed and compared with the pre-timed signal in various traffic conditions. The results show that the proposed control logic works well in both the free-flow condition and the congested condition, can decrease total delay, and can prevent queue overflow.

17. Key Words	18. Distribution Statement
Connected Vehicle, Adaptive Signal Control, Queue Estimation, Discrete Wavelet Transform	No restrictions. This document is available to the public through NTIS: National Technical Information Service Alexandria, Virginia 22312 http://www.ntis.gov

19. Security Classif. (of this report)	20. Security Classif. (of this page)	21. No. of Pages	22. Price
Unclassified	Unclassified	84	

Form DOT F 1700.7 (8-72) **Reproduction of completed page authorized**

ENHANCED ADAPTIVE SIGNAL CONTROL USING DEDICATED SHORT-RANGE COMMUNICATIONS

by

Yunlong Zhang
Assistant Professor
Texas A&M University

and

Kamonthep Tiaprasert
Graduate Research Assistant
Texas A&M University

Report SWUTC/14/600451-00010-1

Sponsored by the
Southwest Region University Transportation Center

May 2014

TEXAS A&M TRANSPORTATION INSTITUTE
College Station, Texas 77843-3135

DISCLAIMER

The contents of this report reflect the views of the authors, who are responsible for the facts and the accuracy of the information presented herein. This document is disseminated under the sponsorship of the U.S. Department of Transportation University Transportation Centers Program in the interest of information exchange. Mention of trade names or commercial products does not constitute endorsement or recommendation for use.

ACKNOWLEDGMENTS

The authors recognize that support for this research was provided by a grant from the U.S. Department of Transportation University Transportation Centers Program to the Southwest Region University Transportation Center, which is funded 50 percent with general revenue funds from the State of Texas.

EXECUTIVE SUMMARY

Connected vehicle (CV) technology is considered a promising way to collect real-time individual vehicle data such as traffic count, speed, and location. Unlike loop detectors, CV technology can gather data at various points along the road. Such data are essential for traffic management systems. Cost-wise, CV technology is effective because it can be deployed on a large scale with less construction and maintenance costs. However, there are difficulties with the low penetration ratio. Vehicles equipped with sensor devices are generally fewer than vehicles without it. As a result, traffic data retrieved from CVs might not have satisfactory accuracy. Therefore, some estimation algorithms are needed to attain accurate traffic data from the CV data. New innovative techniques need to be developed for CVs. On the other hand, adaptive signal control, considered to be very effective in decreasing delay time from pre-timed plans, is also an important contribution to traffic management systems. With the new source of data, new adaptive signal logic must be developed. Therefore, methodologies that can accurately estimate traffic data from CVs and adaptive signal control logic for traffic data are important to not only traffic management systems but traveler information. These methodologies can play important roles in state-of-the-art research and practical applications.

This research began with a review of existing traffic sensors (including CV), their advantages, and their disadvantages. The literature review also examined existing adaptive signal control logics and programs, and adaptive signal control with CV.

This project was divided into three major parts:

- Firstly, researchers proposed applying a coordination system with multi-class macroscopic modeling. The results implied that a multi-class cell transmission model can decrease total delay and stop time when there is free-flow speed variation by accurately predicting arrival time and platoon dispersion.
- Secondly, the queue estimation algorithm from CV was developed without relying on loop detectors. The numerical results showed that the estimated queue length can reasonably and consistently track the queue data simulated from microscopic simulation, VISSIM.
- Finally, researchers proposed adaptive signal control based on CV data and the algorithm developed in the second part. The proposed adaptive signal control works in two modes:

coordination mode and congestion mode. The objectives of the two modes are different. Coordination mode focuses on providing continuous movement on arterial roads, whereas congestion mode tries to minimize total delay from all approaches and prevent queue spill back. The numerical results implied that adaptive signal control can reasonably switch between the two modes according to traffic conditions from CV data. However, the optimization part of the adaptive signal control should be enhanced further, which is a task for future research.

TABLE OF CONTENTS

LIST OF FIGURES xi
LIST OF TABLES xiv
CHAPTER 1. INTRODUCTION 1
Project Objectives 2
Research Tasks 2
Report Organization 3
CHAPTER 2. LITERATURE REVIEW 5
Traffic Detectors 5
Loop Detectors 5
Alternative Detectors 5
Dedicated Short-Range Communications 6
Traffic Signal Control 6
Types of Signal Control 6
Adaptive Signal Control 7
Delay Minimization Algorithm 8
Delay Minimization Theories 8
Model-Based Delay Minimization 9
Queue Length Estimation from CV 9
Summary 10
CHAPTER 3. METHODOLOGY 11
Coordination Systems with Multi-class Traffic and Macroscopic Modeling 11
Cell Connections 11
Flow Calculation 12
Update of Cell Density by Flow Value 18
Queue Length Estimation Using CV Data 19
Adaptive Signal Control Logic Using CV Data 21
Coordination Systems Mode 23
Congestion Mode 24
CHAPTER 4. RESULTS AND DISCUSSION 27

NUMERICAL Results for M-CTM for Coordination Systems 27
Parameter Calibration 28
Offset Optimization 28
Case 1: Symmetry Composition 29
Case 2: Non-symmetry Composition 33
Numerical Results for Queue Length Estimation Using CV Data 36
Case 1: Fixed Signal Control with Undersaturated Condition 37
Case 2: Fixed Signal Control with Saturated Condition 40
Case 3: Actuated Signal Control with Undersaturated Condition 43
Case 4: Actuated Signal Control with Saturated Condition 45
The Proposed Algorithm with Wavelet Transform 46
Numerical Results for Adaptive Signal Control Logic 55
Case 1: Constant Arrival 56
Case 2: Platoon Arrival 60
CHAPTER 5. CONCLUSIONS AND FUTURE WORK 65
REFERENCES 67

LIST OF FIGURES

Figure 1. Typical function of relative occupancy ratio. 13
Figure 2. Cascading scenario. 14
Figure 3. Merging scenario and its equivalent cascading scenario. 15
Figure 4. Diverging scenario and its equivalent cascading scenario. 17
Figure 5. Illustration of non-queued vehicles and queued vehicles. 20
Figure 6. Flowchart of proposed adaptive signal control. 22
Figure 7. Minimum and maximum arrival from CV data. 24
Figure 8. Topology of tested network for S-CTM. 27
Figure 9. Topology of tested network for M-CTM. 28
Figure 10. Number of vehicles of S-CTM after signal optimization. 31
Figure 11. Number of vehicles of M-CTM after optimizing offset. 32
Figure 12. Number of vehicles of S-CTM after signal optimization. 34
Figure 13. Number of vehicles of M-CTM after optimizing offset. 35
Figure 14. Isolated intersection used in queue length estimation. 37
Figure 15. Estimated queue length of proposed algorithm when penetration ratio is 30 percent. 38
Figure 16. Estimated queue length of Comert's algorithm when penetration ratio is 30 percent. 38
Figure 17. Estimated queue length of proposed algorithm when penetration ratio is 50 percent. 39
Figure 18. Estimated queue length of Comert's algorithm when penetration ratio is 50 percent. 39
Figure 19. Estimated queue length of proposed algorithm when penetration ratio is 80 percent. 40
Figure 20. Estimated queue length of Comert's algorithm when penetration ratio is 80 percent. 40
Figure 21. Estimated queue length of proposed algorithm when penetration ratio is 30 percent. 41
Figure 22. Estimated queue length of Comert's algorithm when penetration ratio is 30 percent. 41
Figure 23. Estimated queue length of proposed algorithm when penetration ratio is 50 percent. 42
Figure 24. Estimated queue length of Comert's algorithm when penetration ratio is 50 percent. 42

Figure 25. Estimated queue length of proposed algorithm when penetration ratio is 80 percent. 43
Figure 26. Estimated queue length of Comert's algorithm when penetration ratio is 80 percent. 43
Figure 27. Estimated queue length of proposed algorithm when penetration ratio is 30 percent. 44
Figure 28. Estimated queue length of proposed algorithm when penetration ratio is 50 percent. 44
Figure 29. Estimated queue length of proposed algorithm when penetration ratio is 80 percent. 45
Figure 30. Estimated queue length of proposed algorithm when penetration ratio is 30 percent. 45
Figure 31. Estimated queue length of proposed algorithm when penetration ratio is 50 percent. 46
Figure 32. Estimated queue length of proposed algorithm when penetration ratio is 80 percent. 46
Figure 33. Wavelet transform level 1 of estimated queue length in case 1: fixed signal control with undersaturated condition. 47
Figure 34. Wavelet transform level 2 of estimated queue length in case 1: fixed signal control with undersaturated condition. 48
Figure 35. Wavelet transform level 3 of estimated queue length in case 1: fixed signal control with undersaturated condition. 48
Figure 36. Wavelet transform level 1 of estimated queue length in case 2: fixed signal control with saturated condition. 49
Figure 37. Wavelet transform level 2 of estimated queue length in case 2: fixed signal control with saturated condition. 49
Figure 38. Wavelet transform level 3 of estimated queue length in case 2: fixed signal control with saturated condition. 50
Figure 39. Wavelet transform level 1 of estimated queue length in case 3: actuated signal control with undersaturated condition. 50
Figure 40. Wavelet transform level 2 of estimated queue length in case 3: actuated signal control with undersaturated condition. 51
Figure 41. Wavelet transform level 3 of estimated queue length in case 3: actuated signal control with undersaturated condition. 51
Figure 42. Wavelet transform level 1 of estimated queue length in case 4: actuated signal control with saturated condition. 52
Figure 43. Wavelet transform level 2 of estimated queue length in case 4: actuated signal control with saturated condition. 52
Figure 44. Wavelet transform level 3 of estimated queue length in case 4: actuated signal control with saturated condition. 53

Figure 45. Root mean square error of queue length estimation in case 1: fixed signal control with undersaturated condition 53
Figure 46. Root mean square error of queue length estimation in case 2: fixed signal control with saturated condition..... 54
Figure 47. Root mean square error of queue length estimation in case 3: actuated signal control with undersaturated condition. 54
Figure 48. Root mean square error of queue length estimation in case 4: actuated signal control with saturated condition..... 55
Figure 49. Test network for adaptive signal control logic. 56
Figure 50. Green time for main arterial road of intersection 1 in congestion condition..... 57
Figure 51. Green time for minor road of intersection 1 in congestion condition..... 58
Figure 52. Green time for main arterial road of intersection 2 in congestion condition..... 58
Figure 53. Green time for minor road of intersection 2 in congestion condition. 59
Figure 54. Offset of intersection 1 in congestion condition..... 59
Figure 55. Offset of intersection 2 in congestion condition..... 60
Figure 56. Platoon arrival input for case 2: platoon arrival. 61
Figure 57. Green time for main arterial road of intersection 1 in platoon arrival case. 62
Figure 58. Green time for minor road of intersection 1 in platoon arrival case. 62
Figure 59. Green time for main arterial road of intersection 2 in platoon arrival case..... 63
Figure 60. Green time for minor road of intersection 2 in platoon arrival case. 63
Figure 61. Offset of intersection 1 in platoon arrival case..... 64
Figure 62. Offset of intersection 2 in platoon arrival case..... 64

LIST OF TABLES

Table 1. Calibrated parameters for S-CTM. 29
Table 2. Calibrated parameters for M-CTM. 30
Table 3. Optimal offsets and delay from CORSIM. 30
Table 4. Calibrated parameters for S-CTM. 33
Table 5. Calibrated parameters for M-CTM. 33
Table 6. Optimal offsets and delay from CORSIM. 33
Table 7. Optimal delay and signal plans from case 1 with free-flow condition. 57
Table 8. Optimal delay and signal plans from case 1 with congestion condition. 57
Table 9. Optimal delay and signal plans from case 2. 61

CHAPTER 1. INTRODUCTION

Conflicting flow at urban intersections has always been a problem for traffic management. To ensure safe and smooth traffic flow in the city, signal control is commonly employed at intersections. However, without a good signal timing plan and adequate traffic data, a traffic signal may not serve its purpose or may even cause unnecessary delays and congestion. Development of innovative signal timing strategies based on accurate and comprehensive data in a real-time environment is critical to a sustainable transportation system.

One of the practical limitations that traffic engineers have to overcome is a lack of traffic data for certain advanced control strategies for a large area. Most conventional detectors such as loop detectors are fixed-point detectors and are too costly to install to cover a sufficient area in a large-scale network. On the traffic flow modeling side, one limitation is a single-class macroscopic model. Most macroscopic models are single class and cannot accurately predict traffic states when there is a mixture of vehicles with different speeds. On the other hand, microscopic models are multi-class in nature but may be too computationally expensive to be practical in some applications that require fast simulation. One example is a failure to reproduce platoon dispersion, which occurs when heterogeneous vehicles drive along a signalized arterial. A single-class model, such as the single-class cell transmission model (S-CTM), is unable to predict an approaching platoon of vehicles to a downstream intersection accurately. As a result, a signal timing plan obtained from a single-class model may cause unnecessary delay due to faster-than-average-speed vehicles.

To overcome the aforementioned limitations, connected vehicle (CV) technology with dedicated short-range communications (DSRC) and a multi-class macroscopic model are proposed. With the emergence of advanced telecommunications such as DSRC, an equipped vehicle can act as a vehicle probe and collects data not just in the temporal domain but in the spatial domain. DSRC's implementation is also cost effective, which is promising for future system deployment. Because of DSRC's differences in collecting traffic data, a new algorithm needs to be developed to estimate traffic data from DSRC data to maximize their potential. The obtained data in the spatial domain also enable the use of a new signal control strategy, which is expected to be more effective than existing ones. For a heterogeneous traffic flow, there is a need

for a multi-class macroscopic model to find optimal signal timing. The computational complexity of the model should not be compromised with the increasing accuracy.

PROJECT OBJECTIVES

The objectives of this research project are to:

- Review current adaptive signal control algorithms and the current version of the DSRC standard to better understand technical possibilities and constraints.
- Develop a new adaptive signal control logic that uses DSRC as the primary data collection method.

RESEARCH TASKS

The research team performed the following tasks to meet the objectives:

- **Literature review:** This task involved a literature review of papers and reports concerning DSRC technology and the adaptive signal control algorithm.
- **Control logic development:** New signal timing update algorithms were developed based on newly available vehicle data made possible by DSRC. The necessary techniques, such as queue length estimation based on DSRC, were also developed to enhance adaptive signal control.
- **Performance evaluation:** The developed adaptive control logic and the necessary algorithms such as queue length estimation were evaluated using macroscopic and microscopic simulation tools for various traffic conditions. The performance of the new control logics was compared to the optimal pre-timed signal setting in terms of total delays.
- **Final report:** The procedures, findings, lessons, and algorithms developed were documented. Comments, requirements, and future work to further improve the algorithms were also included.

REPORT ORGANIZATION

The rest of this report is organized as follows:

- **Chapter 2. Literature Review:** This chapter discusses a review of adaptive signal control in past studies.
- **Chapter 3. Methodology:** This chapter proposes a new adaptive signal control for multiple intersections using DSRC data. The application of the multi-class cell transmission model (M-CTM) to improve the performance of signal coordination is presented as well as queue length estimation based on DSRC data.
- **Chapter 4. Results and Discussion:** This chapter validates and verifies the proposed algorithms with the numerical results and simulations. Results from the proposed algorithm and existing methods are compared and evaluated.
- **Chapter 5. Conclusions and Future Work:** This chapter draws conclusions about previous chapters. Findings, suggestions, and suggested future work are included.

CHAPTER 2. LITERATURE REVIEW

This chapter reviews literature from previous research related to this research project. The chapter discusses:

- Traffic detectors.
- Traffic signal control.
- A delay minimization algorithm.

TRAFFIC DETECTORS

Loop Detectors

Traffic data are essential to manage traffic effectively. However, all vehicle detectors have their limitations. The most popular detector is a loop detector. Though most commonly used in research and algorithms because loop detectors provide high accuracy, they have cost issues. First, the construction cost is relatively high, and installation damages the pavement. Second, maintenance costs are also high, and maintenance means re-digging the pavement to fix it. One of the major limitations in terms of data collection is that though temporal data are collected, loop detectors are point detectors. In order to get traffic data along a spatial domain, many loop detectors would need to be installed, which would be cost prohibitive and thus virtually impossible.

Alternative Detectors

To respond to the shortcomings of loop detectors, alternative methods of detection are being sought to be more user friendly and cheaper to construct and maintain. Video detection has been gotten attention due to the relatively low cost and wide-area coverage. However, it has accuracy problems. For example, for small vehicles and/or night time, its accuracy may lessen. There are also certain angles where video might not be able to distinguish vehicles. Video also has maintenance issues.

Other detection methods, such as magnetometer and radar, have the same problem with reliability and accuracy, though for different technical reasons. For example, a cellular probe may acquire large-scale traffic information, but its accuracy suffers from the large coverage of

cell-base stations. A cellular probe detection also cannot separate pedestrians using cell phones from vehicles with cell phones.

For more information regarding cellular probes, please see literature by Work et al. [1], Bayen et al. [2], Pattara-Atikom et al. [3], Sohn and Kim [4], Meyer [5], Amin et al. [6], and Cheng et al. [7].

Dedicated Short-Range Communications

Recently, DSRC and CVs [8–11] have been considered the detector of the future. Using advanced technology in wireless communication, moving vehicles can exchange traffic information with each other and with infrastructure along a roadside. This, along with measurement equipment, allows traffic data to be collected from technology-equipped probe vehicles. Individual vehicle data such as location, speed, and acceleration are collected in real time and cover a large area. Wireless communication also transfers the traffic data to be used in traffic signal control from the vehicle to the infrastructure. This detection system also has lower installation and operation costs. The advantages of CVs are cost-effectiveness, reliability, high accuracy potential, and delivery of most, if not all, desired traffic data. However, a low penetration ratio can decrease accuracy, so CVs need estimation algorithms. The U.S. Department of Transportation has sponsored several projects concerning CVs. For example, the Connected Vehicle Test Bed has been opened to support ongoing research in a real-world environment [12]. Also, CarTel has developed a mobile sensor computing system from probe vehicles [13].

TRAFFIC SIGNAL CONTROL

Types of Signal Control

Signal control logic is as important as traffic data collection. The three types of signal control are:

- **Pre-timed control:** a fixed-time plan that repeats the preset signal plan created from historical data. Pre-timed control cannot deal with a change in traffic patterns and fluctuations.

- **Actuated control:** works with detectors at the intersection. Green time is extended if there are vehicles in the respective approaches until there is no vehicle left or the cumulative green time reaches its upper bound.
- **Adaptive signal control:** uses real-time traffic information to choose the optimal signal plan every few minutes and respond to variations in traffic patterns.

According to the Federal Highway Administration (FHWA), the implementation of adaptive signal control is less than 1 percent [14]. FHWA wants to replace the old-generation signal system with adaptive signal control. However, there are only a few studies of adaptive signal control's long-term benefits, according to the National Cooperative Highway Research Program [15]. Skabardonis and Gomes [16] conducted one study of adaptive signal control's effectiveness, including a comparison of adaptive signal programs.

Adaptive Signal Control

Adaptive signal control systems using loop detectors include:

- The Split, Cycle, and Offset Optimization Technique (SCOOT) [17].
- The Sydney Coordinated Adaptive Traffic System (SCATS) [18].
- The Optimized Policies for Adaptive Control (OPAC) [19].
- The Real-Time Hierarchical Optimizing Distributed Effective System (RHODES) [20].
- InSync [21].

SCOOT and SCATS uses traffic data from loop detectors to coordinate the signal at small time increments by optimizing cycle, offset and split. Unlike SCOOT and SCATS, OPAC does not use a concept of cycle length. Data from loop detector is used to make decision whether to extend or stop the current phase. RHODES and InSync find the optimal signal by decomposing the optimization algorithm into sequences. For RHODES, the sequences are dynamic network loading, network flow control, and intersection control. InSync uses two-level optimization, global and local optimization, to allow continuous movement for main arterials and to allocate green time to minor streets, respectively. These systems have problems during oversaturated conditions since the queue length is longer than the placement of the loop detectors. Thus, queue detection fails to detect the actual demand, and the systems cannot find a good signal setting for such situations. Another problem is that loop detectors cannot distinguish between a normal

queue and a queue due to spill back from a downstream intersection. As a result, these systems cannot solve such situations.

There is some research in which adaptive signal control is based on CV. For example, Cai et al. [22] used travel times from CV to input the signal control. He et al. [23] proposed platoon-based arterial multimodal signal control with online data (PAMSCOD). However, none of these research projects used queue-based adaptive signal control. Some researchers state the benefit of using queue length as an input to signal control, but the difficulty of developing a queue length estimation algorithm for non-fixed signal control limits queue length's usefulness.

DELAY MINIMIZATION ALGORITHM

Delay Minimization Theories

The two well-known theories to minimize delay are Webster's equation [24] and a bandwidth-based algorithm developed by Brook and Little.

Webster's equation is:

$$C_{opt} = \frac{1.5L + 5}{1 - \sum_{1}^{n} \left(v_i / s_i \right)_{cr}} \tag{2.1}$$

Where:

C_{opt} = the optimal cycle length for minimizing delay.

L = the sum of lost time of all phases.

$\left(v_i / s_i \right)_{cr}$ = the critical flow ratio of phase i.

Webster's equation calculates the optimal cycle length, which is used to find the green time allocated to each approach. On the other hand, the bandwidth-based algorithm is used to find the optimal offset for continuous movement for arterial roads. Green time for the coordination system is set so that arriving vehicles from two directions can get green time immediately. However, the bandwidth-based algorithm does not consider residual queue and multi-class traffic. The bandwidth-based algorithm also does not find optimal cycle length or

phase sequences. Moreover, the cycle lengths of all intersections in the system need to be the same. Minor streets tend to get more congestion due to their lesser priority.

Model-Based Delay Minimization

To overcome limitations from the aforementioned theories, model-based optimization was developed. There are two types of traffic modeling: macroscopic and microscopic modeling. For real-time signal control, a macroscopic model is preferable because it has lower computational time. A popular macroscopic model, S-CTM [25, 26] has been applied to signal optimization and has proved to be effective in decreasing total delay time [27].

Queue Length Estimation from CV

Queue length estimation may be divided into two major approaches: the last probe vehicle location and shockwave theory (or vehicle trajectory). Queue length estimation from CVs was first proposed by Comert and Cetin [28, 29, 30, 31]. The research provided an analytical model to evaluate the queue length estimation's performance based on the penetration ratio value. By using the last location of the probe vehicle in the queue and prior knowledge of the penetration ratio, the expectation of queue length can be estimated:

$$E(N \mid L_p = l_p) = \sum_{n=l_p}^{\infty} n \frac{\left[(1-p)\right]^n P(N=n)}{\sum_{k=l_p}^{\infty} \left[(1-p)\right]^k P(N=k)}, \quad \text{for } l_p \geq 1 \tag{2.2}$$

Where:

$N =$ the actual total queue length.

$L_p =$ the location of the last probe vehicle in the queue.

$p =$ the penetration ratio.

$P(N) =$ the probability function of the total actual queue length.

However, as noted by Cheng et al. [32], the methods requires a signal timing as a basic input but the signal timing information may not always be available. The queue length estimation algorithm was developed by using shockwave theory. The vehicle trajectory can be reconstructed from CV. The signal timing is also detected by critical points from the shockwave-based model. Though the second approach requires less basic inputs, the relationship or impact of the

penetration ratio to the accuracy of queue length estimation is not given. The other method of queue length estimation using shockwave theory is used by Izadpanah et al. [33], Hao and Sun [34], and Sun and Ban [35].

Even though some queue length estimations have been proposed, most research has been limited to fixed-time signals. In conclusion, no queue length algorithm has been proposed or verified against signal timing other than a fixed-time signal, much less adaptive signal control.

SUMMARY

Even though some research has been performed on adaptive signal control or CVs separately, only a few studies have examined adaptive signal control using CV data [36, 37]. None of these studies set traffic signals based on queue estimation from CV data. Because queue length is one of the best indicators in measures of effectiveness and the objective function of signal optimization, it is essential that queue length be obtained without relying on loop detectors. Queue information is also useful to many applications in traffic information and management. No studies consider spill-back prevention or treat incoming vehicles and in-queue vehicles separately. Therefore, to maximize the capability of both adaptive signal control and CV data, new adaptive signal logic based on queue length and incoming demand needs to be developed.

CHAPTER 3. METHODOLOGY

This chapter describes the new proposed algorithms and is divided into three parts:

- Coordination systems with multi-class traffic and macroscopic modeling.
- Queue length estimation using CV data.
- The adaptive signal control logic using CV data.

COORDINATION SYSTEMS WITH MULTI-CLASS TRAFFIC AND MACROSCOPIC MODELING

One of the most important aspects of a coordination system is how it predicts the arrival time to an intersection accurately in order to enable continuous movement. Most coordination systems assume traffic is single class with a single free-flow speed to derive arrival time. However, in practice, drivers drive at different desired speeds, which causes platoon dispersion in signalized road networks. To provide continuous movement through multiple intersections, accurate platoon prediction is needed. Most microscopic models are multi-class in nature, but their high complexity is not suitable for adaptive signal control. Most macroscopic models are either single-class or freeway-only models. However, multi-class cell transmission models can predict platoon dispersion accurately, are macroscopic with fast computation times, and are applicable to signalized networks, so multi-class cell transmission models are suitable for adaptive signal control in coordination mode [38]. Multi-class cell transmission models are therefore applied to find an optimal coordination system with multi-class traffic.

Cell Connections

First, time is discretized into time intervals. The size of the time interval is determined by how frequent the model updates the traffic state. In signalized systems, the time interval should be small enough to capture the dynamics of the system. After the time interval is decided, a cell's length can be calculated by the distance that the fastest vehicle in the system can travel in one time interval or the free-flow speed of the fastest class multiplied by the size of the time interval. Then the road is divided into smaller cells by the cell's length. Vehicles are classified by their free-flow speeds from the slowest class 1 to the fastest class M.

Flow Calculation

After the road network is represented by cell connections, the flow value is calculated to update density. First, the sending capability of the beginning or upstream cell, *Bg*, is calculated:

$$s_{Bg}(t) = \min\left\{\sum_{m=1}^{M}\left[\tilde{l}_m a_{Bg,m}(t)\right] + \sum_{m=1}^{M}\left[\tilde{v}_m \tilde{l}_m b_{Bg,m}(t)\right], q_E(t)\right\} \quad (3.1)$$

Where:

M = the total number of vehicle classes in consideration.

m = the vehicle class index $(m = 1,\ldots,M)$.

$\tilde{v}_m$ = the normalized free-flow speed of class-m vehicles with respect to the maximum free-flow speed of class-M vehicles ($\tilde{v}_M = 1$ and $\tilde{v}_m \in [0.5,1]$).

$\tilde{l}_m$ = the normalized length of each class-m vehicle with respect to the length of class-M vehicles.

$q_E(t)$ = the maximum flow capacity of the link connecting upstream cell Bg to downstream cell E at time slot t.

$a_{Bg,m}(t)$ = the number of head-of-cell vehicles of class m in cell D at time slot t.

$b_{Bg,m}(t)$ = the number of end-of-cell vehicles of class m in cell D at time slot t.

The two types of receiving capability of the ending cell or downstream cell, *E*, is calculated by:

$$\tilde{r}_E(t) = \min\left\{q_E(t), \delta_E\left[c_E - \sum_{m=1}^{M}\left(\tilde{l}_m \psi_{E,m}(t) n_{E,m}(t)\right)\right]\right\} \quad (3.2)$$

$$\tilde{r}_E^*(t) = \tilde{r}_E(t) - s_{Bg,a}(t) \quad (3.3)$$

Where:

$\psi_{E,m}(t)$ = the relative occupancy ratio of class-m vehicles in downstream cell E at time slot *t*. The example function is shown in Figure 1.

$\tilde{r}_E(t)$ = the relative receiving capability of downstream cell E at time slot t.

c_E = the capacity of downstream cell E (defined as the maximum number of vehicles of reference class M that can be stored in the cell).

δ_E = the wave coefficient of downstream cell E.

$r_E^*(t)$ = the receiving capability after deducting the sending capability due to head-of-cell vehicles.

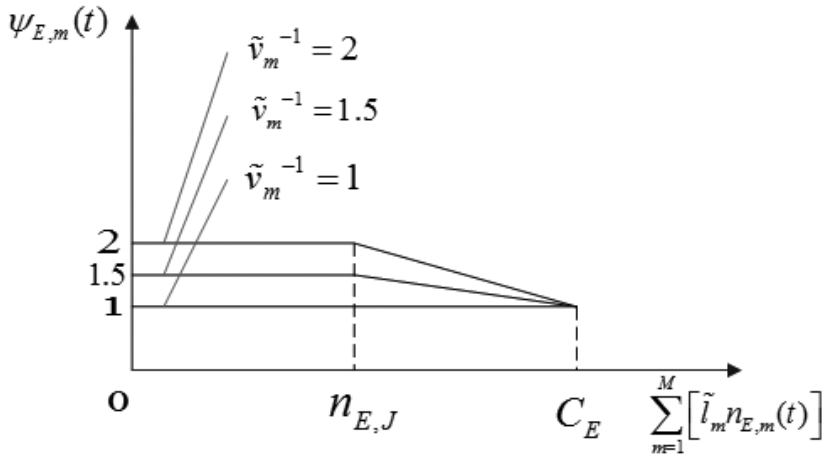

Figure 1. Typical function of relative occupancy ratio.

The flow value for links is updated depending on the type of connection. There are three scenarios:

- Cascading scenario.
- Merging scenario.
- Diverging scenario.

Merging and diverging scenarios are special cases of cascading scenarios and thus can be reduced and calculated as two simple cascading scenarios.

Cascading Scenario

This scenario is the simplest scenario, with only one beginning cell and one ending cell, as shown in Figure 2**Error! Reference source not found.**.

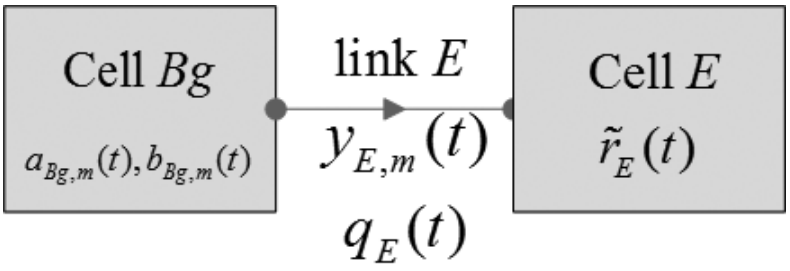

Figure 2. Cascading scenario.

The flow calculation can be divided into three cases:

1. The ending cell cannot receive all head-of-cell vehicles from the beginning cell:

$$s_{Bg,a}(t) > \tilde{r}_E(t) \tag{3.4}$$

Flows can be obtained from:

$$\sum_{m=1}^{M} y_{E,m}(t) = \tilde{r}_E(t) \tag{3.5}$$

$$y_{E,m}(t) = \frac{\tilde{v}_m a_{Bg,m}(t)\tilde{r}_E(t)}{\sum_{m=1}^{M}\left[\tilde{v}_m \tilde{l}_m a_{Bg,m}(t)\right]} \tag{3.6}$$

2. The ending cell can receive all vehicles from the beginning cell including both head-of-cell vehicles and end-of-cell vehicles:

$$s_{Bg,a}(t) \le \tilde{r}_E(t) \tag{3.7}$$

$$s_{Bg,b}(t) \le \tilde{r}_E^*(t) \tag{3.8}$$

Flows can be calculated from:

$$y_{E,m}(t) = a_{Bg,m}(t) + \tilde{v}_m b_{Bg,m}(t) \tag{3.9}$$

3. The downstream cell can receive all head-of-cell vehicles but not all end-of-cell vehicles from the upstream cell:

$$s_{Bg,a}(t) \le \tilde{r}_E(t) \tag{3.10}$$

$$s_{Bg,b}(t) > \tilde{r}_E^*(t) \tag{3.11}$$

Flows can be calculated from:

$$\sum_{m=1}^{M} y_{E,m}(t) = \sum_{m=1}^{M} a_{Bg,m}(t) + \tilde{r}_E^*(t) \tag{3.12}$$

$$y_{E,m}(t) = a_{Bg,m}(t) + \frac{\tilde{v}_m b_{Bg,m}(t)\tilde{r}_E^*(t)}{\sum_{m=1}^{M}\left[\tilde{v}_m \tilde{l}_m b_{Bg,m}(t)\right]} \tag{3.13}$$

Merging Scenario

Figure 3. shows the topology for the merging scenario and its reduction to two cascading scenarios. The merging proportion of link *i*, p_i is defined as a proportion of the relative receiving capability for upstream cell *i* when the downstream cell cannot receive all vehicles from both upstream cells.

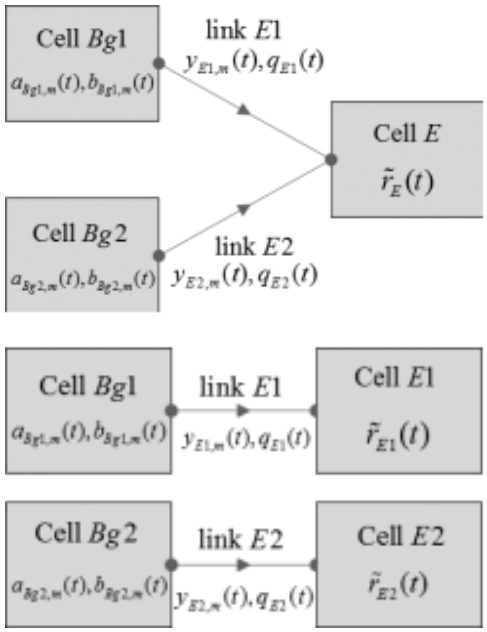

Figure 3. Merging scenario and its equivalent cascading scenario.

In order to reduce the merging scenario to simpler cascading scenarios, the relative receiving capability of downstream cell $\tilde{r}_{E1}(t)$ and $\tilde{r}_{E2}(t)$ is calculated:

1. The downstream cell can receive both head-of-cell vehicles and end-of-cell vehicles from both beginning cells:

$$s_{Bg1}(t) + s_{Bg2}(t) \leq \tilde{r}_E(t) \tag{3.14}$$

   In this case, the relative receiving capability of both equivalent downstream cells is equal to their respective sending capability:

$$\tilde{r}_{E1}(t) = s_{Bg1}(t) \tag{3.15}$$

$$\tilde{r}_{E2}(t) = s_{Bg2}(t) \tag{3.16}$$

2. Only one of the upstream cells has its sending capability greater than its merging proportion of the receiving capability. The assumption is that the exceeding upstream cell is *Bg*1:

$$s_{Bg1}(t) + s_{Bg2}(t) > \tilde{r}_E(t) \tag{3.17}$$

$$s_{Bg1}(t) > p_1 \tilde{r}_E(t) \tag{3.18}$$

$$s_{Bg2}(t) \leq p_2 \tilde{r}_E(t) \tag{3.19}$$

   In this case, only the upstream cell *Bg*2 can forward all its vehicles to the downstream cell. The upstream cell *Bg*1 can forward its vehicles equal to the remaining capacity after deduction from *Bg*1:

$$\tilde{r}_{E1}(t) = \tilde{r}_E(t) - s_{Bg2}(t) \tag{3.20}$$

$$\tilde{r}_{E2}(t) = s_{Bg2}(t) \tag{3.21}$$

3. Both upstream cells have their sending capability greater than their merging proportion of the receiving capability:

$$s_{Bg1}(t) + s_{Bg2}(t) > \tilde{r}_E(t) \tag{3.22}$$

$$s_{Bg1}(t) > p_1 \tilde{r}_E(t) \tag{3.23}$$

$$s_{Bg2}(t) > p_2 \tilde{r}_E(t) \tag{3.24}$$

In this case, no upstream cell can forward all its vehicles to the downstream cell. It can forward its vehicles proportional to its merging proportion:

$$\tilde{r}_{E1}(t) = p_1 \tilde{r}_E(t) \tag{3.25}$$

$$\tilde{r}_{E2}(t) = p_2 \tilde{r}_E(t) \tag{3.26}$$

After $\tilde{r}_{E1}(t)$ and $\tilde{r}_{E2}(t)$ are found, the merging scenario can be reduced to two simple cascading scenarios. Then $y_{E1,m}(t)$ and $y_{E2,m}(t)$ are calculated through cascading flow equations 3.4 through 3.13.

Diverging Scenario

This topology has one upstream cell and two downstream cells, as shown in Figure 4.

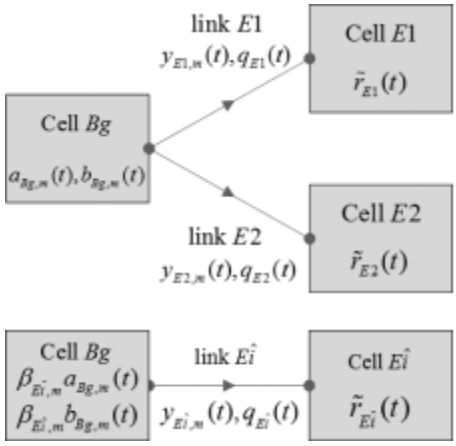

Figure 4. Diverging scenario and its equivalent cascading scenario.

By assuming head-of-line blocking, flow is stopped when one of the downstream cells reaches its capacity. The breaking proportion $\beta_{Ei,m}$ is defined as a proportion of vehicle type *m* from upstream cell *i* where $\beta_{E1,m} + \beta_{E2,m} = 1, \forall m$. The breaking proportions are given from

empirical data or dynamic traffic assignment reflecting how many vehicles want to go to path *E1* and *E2*.

For the equivalent cascading scenario, the downstream cell $E\hat{i}$ that reaches its capacity is found first by:

$$\hat{i} = \arg\min_{i=1,2} \left\{ \frac{\tilde{r}_{Ei}(t)}{\sum_{m=1}^{M} \left[\beta_{Ei,m} \tilde{l}_m \left(a_{Bg,m}(t) + \tilde{v}_m b_{Bg,m}(t) \right) \right]} \right\} \tag{3.27}$$

Then, assuming $\hat{i} = 1$, the flow from upstream cell *Bg* to downstream cell *E1* can be calculated by a simple cascading scenario using the breaking proportion:

1. Compute $s_{Bg}(t)$ with equation 3.1 by letting $a_{Bg,m}(t) = \beta_{E1,m} * a_{Bg,m}(t)$ and $b_{Bg,m}(t) = \beta_{E1,m} * b_{Bg,m}(t)$.

2. Use cascading flow equations 3.4 through 3.13 to calculate $y_{E1,m}(t)$ with the $s_{Bg}(t)$ from step 1 and $\tilde{r}_E(t) = \tilde{r}_{E1}(t)$.

3. Finally, $y_{E2,m}(t)$ is calculated by:

$$y_{E2,m}(t) = \frac{\beta_{E2,m}}{\beta_{E1,m}} y_{E1,m}(t) \tag{3.28}$$

Update of Cell Density by Flow Value

After the flow value for the links is calculated, the density of cells is updated by:

$$a_{D,m}(t+1) = n_{D,m}(t) - \sum_{k \in \{\text{output link(s) of } D\}} y_{k,m}(t) \tag{3.29}$$

$$b_{D,m}(t+1) = \sum_{k \in \{\text{input link(s) of } D\}} y_{k,m}(t) \tag{3.30}$$

$$n_{D,m}(t+1) = a_{D,m}(t+1) + b_{D,m}(t+1) \tag{3.31}$$

Where:

$a_{D,m}(t)$ = the number of head-of-cell vehicles of class m in cell D at time slot t.

$b_{D,m}(t)$ = the number of end-of-cell vehicles of class m in cell D at time slot t.

$n_{D,m}(t)$ = the number of class-m vehicles in cell D at time slot t.

$y_{k,m}(t)$ = the flow of class m on link k at time slot t.

QUEUE LENGTH ESTIMATION USING CV DATA

Unlike data from loop detectors, data from CV are in both the time and spatial domains, so CV data can predict long queue length without additional replacement cost. The proposed algorithm assumes the distance and instantaneous speed of equipped individual vehicles can be obtained from CV data. A penetration ratio is known and is an input, though it might be estimated from CV data. The algorithm is also developed without cooperating data from other sources such as loop detectors.

As shown in Figure 5., detected vehicles are classified into two types—non-queued vehicles and queued vehicles—by their instantaneous speed. Stopping speed or crawling speed is defined as a speed that vehicles move waiting in a queue. This speed does not need to be zero, but it should be a very small number. An individual vehicle with a speed from CV data lower than the stopping speed is classified as a queued vehicle. On the other hand, an individual vehicle with a speed from CV data greater than the stopping speed is classified as a non-queued vehicle.

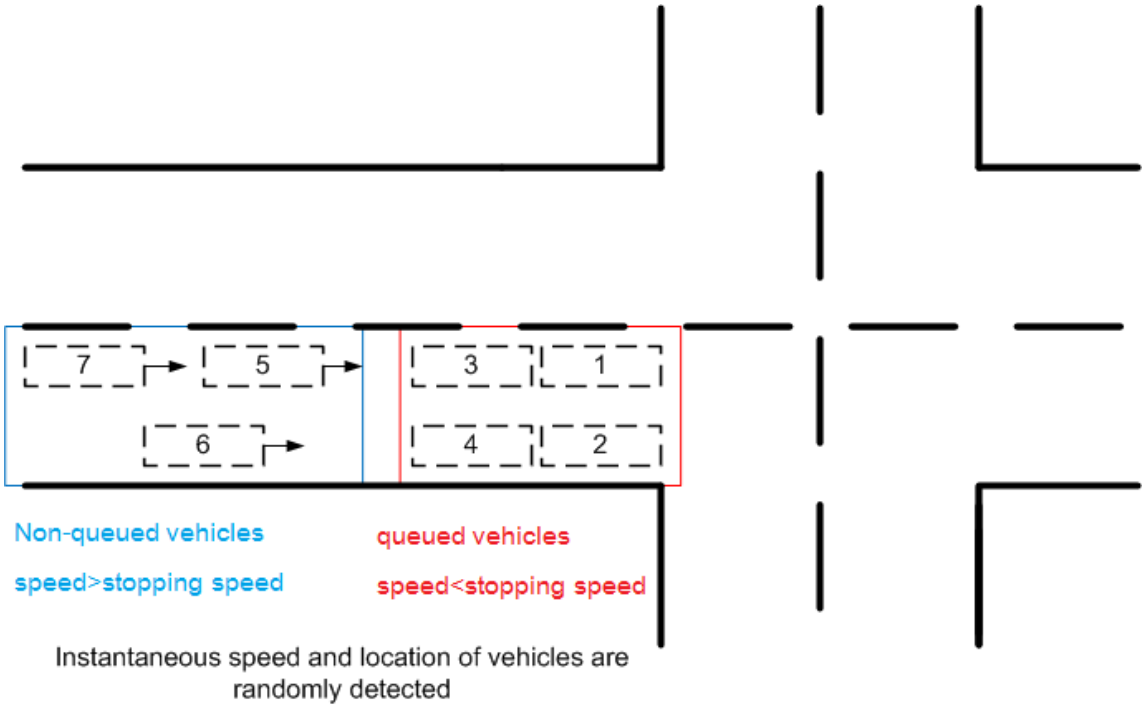

Figure 5. Illustration of non-queued vehicles and queued vehicles.

The range of queue length is found by:

$$\min(Q) \le \hat{Q} \le \max(Q) \tag{3.32}$$

$$I = \max(i), v_i \le v_{stop} \tag{3.33}$$

$$J = \min(j), v_j > v_{stop} \tag{3.34}$$

$$\min(Q) = \left\lceil \frac{s_I}{l} \right\rceil \tag{3.35}$$

$$\max(Q) = \left\lfloor \frac{s_J}{l} \right\rfloor \tag{3.36}$$

Where:

v_1, v_2, v_3,… = the detected speeds of individual vehicles.

s_1, s_2, s_3,… = the distance of vehicles i from a downstream intersection.

Because the probability that a vehicle is equipped is a Bernouli distribution and it's independent of each other, the probability of the total number of detected vehicles is a binomial distribution. The probability function is:

$$P(x=k,n=n)=\binom{n}{k}p^{k}(1-p)^{n-k} \tag{3.37}$$

Where:

k = the number of detected vehicles in the queue determined by CV data.

n = the actual number of vehicles in the queue.

p = the penetration ratio.

The estimation of the queue length is found by minimizing the expectation of the mean square of the queue length estimation error:

$$\begin{aligned}\hat{n}_{MSE} &= \arg\min_{\hat{n}}\left\{E\left[\left(\hat{n}-n\right)^{2}\right]\right\}=\arg\min_{\hat{n}}\left\{\frac{\sum_{n=n_{\min}}^{n_{\max}}\left[P(x=k,n)\left(\hat{n}-n\right)^{2}\right]}{\sum_{n=n_{\min}}^{n_{\max}}P(x=k,n)}\right\} \\ &= \arg\min_{\hat{n}}\left\{\sum_{n=n_{\min}}^{n_{\max}}\left[P(x=k,n)\left(\hat{n}-n\right)^{2}\right]\right\},\hat{n}\in I^{+},n_{\min}\le\hat{n}\le n_{\max}\end{aligned} \tag{3.38}$$

Where:

$n_{\min}$ = the number of lanes * min(Q).

$n_{\max}$ = the number of lanes * max(Q).

ADAPTIVE SIGNAL CONTROL LOGIC USING CV DATA

The proposed adaptive signal control logic is developed in two modes:

- The coordination systems mode.
- The congestion mode.

Where traffic conditions are light, adaptive signal control enables continuous movement for vehicles in major arterials with the coordination systems mode. On the other hand, the

congestion mode attempts to minimize queue lengths and prevent queue overflow when traffic is in a congestion state. The flowchart of adaptive signal control is shown in Figure 6.

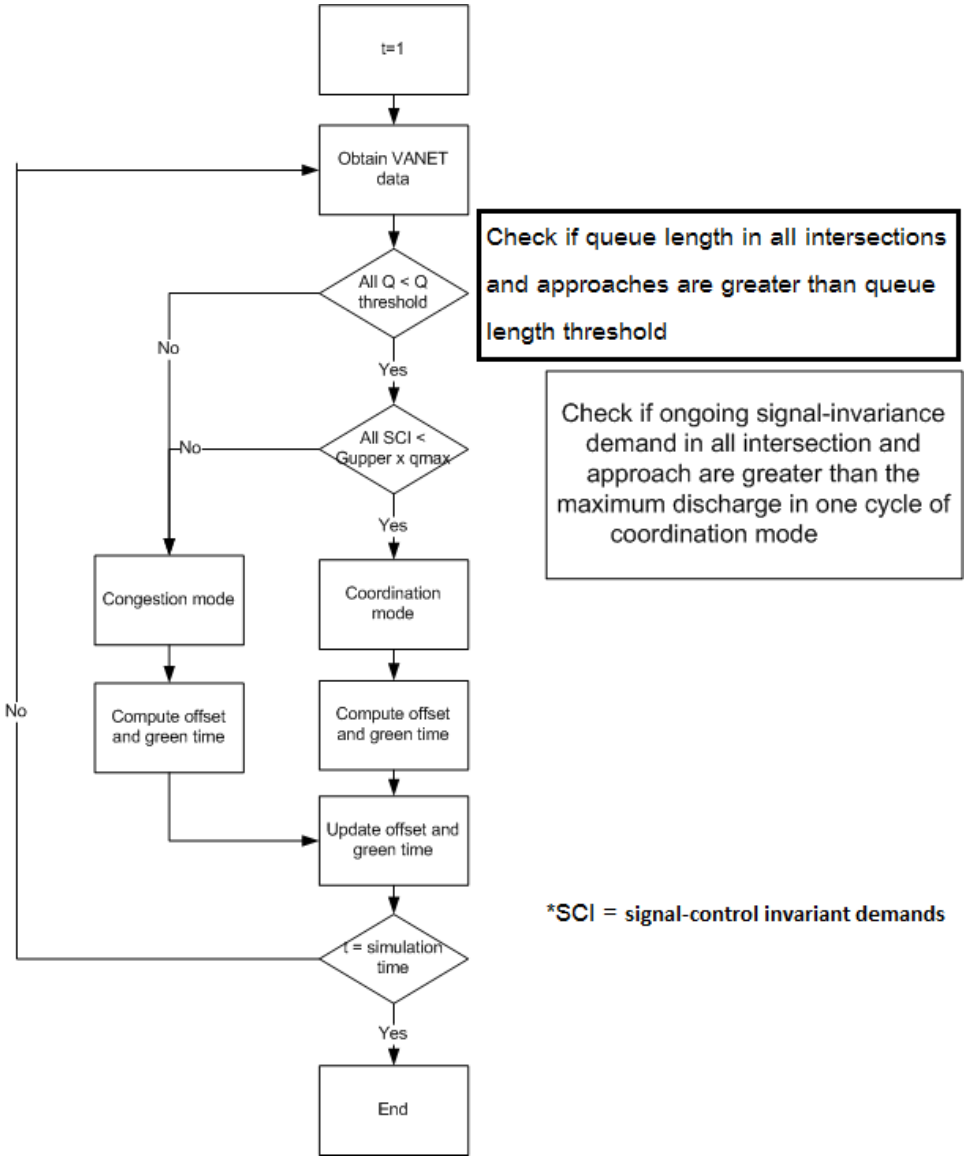

Figure 6. Flowchart of proposed adaptive signal control.

First, CV data are collected, and then queue lengths for all approaches of all intersections are estimated with the algorithm in Chapter 3. From the CV data, non-queued vehicles or signal-control invariant demands (SCI) are also calculated.

The signal control mode is chosen based on the queue lengths and SCI. The condition for the coordination systems mode is that all queue lengths and SCIs are not greater than their queue

length's threshold and maximum available vehicle discharge, as shown in equations 3.39 through 3.41. Otherwise, adaptive signal control works in the congestion mode.

$$\tilde{Q}L_i \le QL_{thres,i}, \forall i \tag{3.39}$$

$$SCI_i \le G_{Max,i} * q_i, \forall i \tag{3.40}$$

$$G_i = \frac{\text{a number of lanes} * \tilde{Q}L_i}{q_i} \tag{3.41}$$

Where:

QL_i = the queue length of approach *i*.

$QL_{thres,i}$ = the threshold of the queue length of approach *i*.

SCI_i = signal control in variant demand of approach *i*.

$G_{upper,i}$ = the maximum green time for approach *i* in seconds.

q_i = the maximum flow rate of approach *i* in vehicles per second.

After the signal control mode is decided, the adaptive signal control calculates the green time and offset for each intersection.

Coordination Systems Mode

In this mode, major arterials and minor roads are treated differently. For major arterial approaches, the green time and offset are calculated:

$$\text{Offset} = \text{minimum arrival} \tag{3.42}$$

$$\text{Green time} = \text{maximum arrival time} - \text{minimum arrival time} \tag{3.43}$$

Figure 7 shows the maximum arrival time and minimum arrival time. Unlike in a bandwidth-based algorithm, a residue queue is taken into account. If a queue is detected, an offset is set to zero by default to allow vehicles in the queue to move without waiting. If no queue is detected, a minimum arrival time is calculated for a detected vehicle at the head of the incoming platoon. The arrival time is calculated by assuming single-class traffic. If traffic is multi-class, M-CTM should be used to find the offset and green time instead.

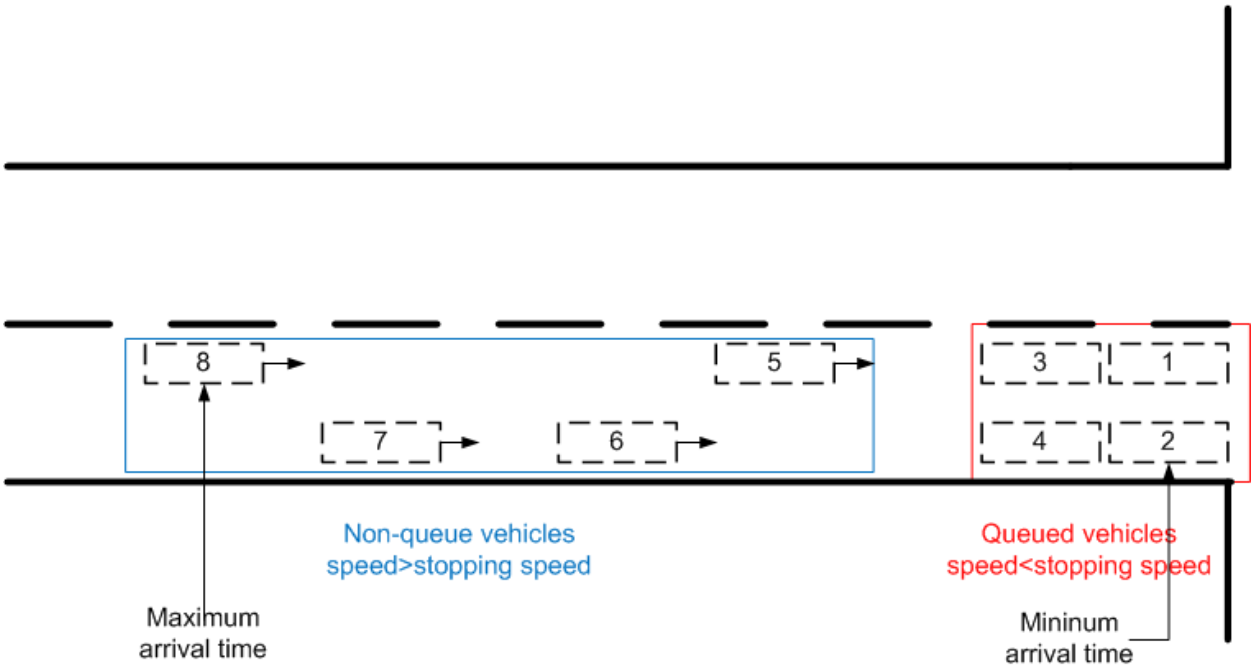

Figure 7. Minimum and maximum arrival from CV data.

For minor streets, the green time is derived from the number of vehicles in the queue divided by the maximum flow rate:

$$G_i = \frac{\text{a number of lanes}*\tilde{Q}L_i}{q_i} \tag{3.44}$$

Congestion Mode

The congestion mode is used when at least one of the queue lengths exceeds the queue length's threshold or total demand is greater than the maximum throughput. The congestion mode tries to prevent queue overflow to the upstream intersection by setting a minimum green time for the downstream intersection, as in equation 3.45. Equation 3.45 sets a maximum green time condition so that green time is not wasted. Equation 3.46 sets a minimum green time condition so that the queue length after green time should be lower than the queue length's threshold. Equation 3.47 then calculates the green time after updating the maximum and minimum green time using equations 3.45 and 3.46.

$$G_{\max,i} = \min\left(G_{upper,i}, \left\lceil \frac{SCI_i + QL_i}{q_i} \right\rceil\right), \forall i \text{ is approach to upstream intersection} \tag{3.45}$$

$$G_{\min,i} = \max\left(G_{lower,i}, \left\lceil \frac{SCI_i + QL_i - QL_{\max,i}}{q_i} \right\rceil \right), \forall i \text{ is approach to downstream intersection} \quad (3.46)$$

$$G_i = \max\left(G_{\min,i}, \min\left(\left\lceil \frac{QL_i * \text{number of lanes}}{q_i} \right\rceil, G_{\max,i} \right) \right) \quad (3.47)$$

The offset in the congestion mode is set so that the approach that needs a green signal the most can go forward first. As a result, the approach that has the biggest G_i will move first.

CHAPTER 4. RESULTS AND DISCUSSION

This chapter provides the numerical results of the algorithms in Chapter 3:

- M-CTM is tested for coordination systems by comparing the minimizing of total delay with S-CTM.
- The queue length estimation algorithm using CV data is verified with microscopic simulation, VISSIM.
- The adaptive signal control logic using CVs is tested on S-CTM against pre-timed signal control.

NUMERICAL RESULTS FOR M-CTM FOR COORDINATION SYSTEMS

In experiment, vehicles have an average free-flow speed of 45 mph. In S-CTM, there is only one class of vehicle, so the free-flow speed of the class is 45 mph. In M-CTM, the free-flow speeds of classes are varied from case to case with different free-flow speed distributions. The test network is an arterial road with three intersections. The first and last intersections are at both ends of the arterial road. The arterial road is 5,740 feet long with four lanes and has the second intersection at a distance of 2,460 feet from the first intersection. The volume is 2,000 vehicles per hour with uniform arrival. The time interval is 5 seconds for both S-CTM and M-CTM. The simulation time is 500 seconds, and the total number of time slots or time intervals is 100. The green time and cycle length are set to be 30 and 60 seconds, respectively. The maximum flow rate of all links and wave propagation of all cells are set to be the same. The topologies of S-CTM and M-CTM are shown in Figure 8 and Figure 9, respectively. A microscopic program, CORSIM [39], is used as a test bed to verify the resultant offset from S-CTM and M-CTM.

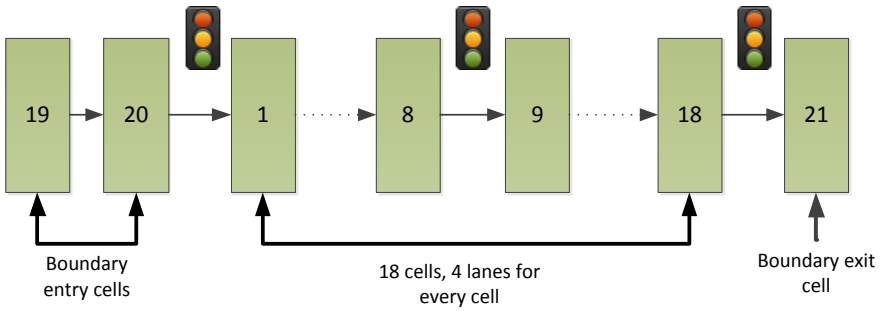

Figure 8. Topology of tested network for S-CTM.

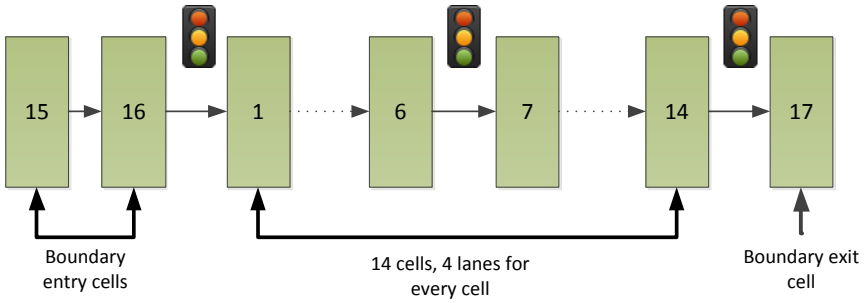

Figure 9. Topology of tested network for M-CTM.

Parameter Calibration

A genetic algorithm is applied to find the necessary parameters of S-CTM and M-CTM. The fitness function is defined as the root mean square error of density:

$$\text{RMSE} = \sqrt{\frac{\sum_{i=1}^{I}\sum_{t=1}^{T}\left(\hat{x}_i(t) - x_i(t)\right)^2}{I * T}} \tag{4.1}$$

Where:

T = the total number of time slots.

I = cells being computed.

$\hat{x}_i(t)$ = the density computed from either S-CTM or M-CTM where $x_i(t)$ is the density simulated from the microscopic mobility model (CORSIM).

The necessary parameters are set as populations that will evolve until the fitness function is minimized. The other settings remain the defaults set by MATLAB.

Offset Optimization

After S-CTM and M-CTM are calibrated with CORSIM's simulated data, total delay is minimized to obtain the optimal offset. The equation for total average delay is:

$$\text{Total delay} = \sum_{t=1}^{100}\sum_{D=1}^{I}\left(n_{D,m}(t) - \sum_{k\in\{\text{output link(s) of } D\}} y_{k,m}(t) \right) * \text{Time interval} \tag{4.2}$$

Where:

Total delay = the total delay experienced by all vehicles in seconds.

I = a number of cells excluding all boundary cells.

Time interval = 5 seconds.

For S-CTM and M-CTM, I equals 18 and 14 cells, respectively.

The offset of intersection 1 is set to zero, and the offset of intersections 2 and 3 are found by optimization. The brute force method is used to find the optimized offset since the genetic algorithm gives unrealistic results in this case. Total delay calculated from S-CTM could be zero, while M-CTM's total delay could not be zero when there is more than one class of vehicle. A delay estimation in M-CTM is done by comparing the traveling time of each class with the ideal traveling time of the fastest class, so the slower classes always causes a delay even in free-flow condition.

Case 1: Symmetry Composition

In this case, there are three classes of 16.5-foot-long vehicles with three different free-flow speeds—60, 45, and 30 mph—with a proportion equaling to 0.2, 0.6, and 0.2, respectively. The calibrated parameters for S-CTM and M-CTM are shown in Table 1 and Table 2. Then the calibrated parameters of S-CTM and M-CTM are used to find the optimal offset. The minimum total delay from S-CTM and M-CTM after signal optimization are zero and 6,356.4 seconds, respectively. The results from CORSIM with the optimal offset from S-CTM and M-CTM are shown in Table 3.

Table 1. Calibrated parameters for S-CTM.

Calibrated Parameters	Lower Bound	Upper Bound	Value after Calibration
Maximum flow rate per lane per time slot	0.23	4.6	2.93
Wave propagation ratio	0.3	1	0.53
Offset for all intersections (time slot)	0	11	11

Table 2. Calibrated parameters for M-CTM.

Calibrated Parameters	Lower Bound	Upper Bound	Value after Calibration
Maximum flow rate per lane per time slot	0.23	4.6	4.177
Wave propagation ratio	0.3	1	0.61
Offsets for all intersections (time slot)	0	11	1
Normalized free-flow speed of vehicle type 2	0.5	1	0.70
Normalized free-flow speed of vehicle type 3	0.5	1	0.50

Table 3. Optimal offsets and delay from CORSIM.

	S-CTM's Offset	M-CTM's Offset
Optimal offset of intersection 1 (seconds)	0	0
Optimal offset of intersection 2 (seconds)	40	40
Optimal offset of intersection 3 (seconds)	30	30
Delay person-minute at intersection 2	322.3	322.3
Control delay at intersection 2 (seconds/vehicle)	14.2	14.2
Queue delay at intersection 2 (seconds/vehicle)	11.3	11.3
Stop time (seconds/vehicle)	10.5	10.5
Delay person-minute at intersection 3	352.5	352.5
Control delay at intersection 3 (seconds/vehicle)	27.5	27.5
Queue delay at intersection 3 (seconds/vehicle)	20.1	20.1
Stop time (seconds/vehicle)	18.9	18.9
Vehicle-hour of delay time	1.71	1.71

As shown in Table 3, optimal offsets from S-CTM, M-CTM, and the bandwidth progression are the same. Slower and faster vehicles are distributed equally, so there is a compromise between them. However, S-CTM fails to reduce and detect delay resulting from platoon dispersion. On the other hand, M-CTM finds stops and delays as CORSIM does in Table 3. It is just coincidence in the case of symmetry composition.

Examples of S-CTM and M-CTM's density after offset optimization are shown in Figure 10 and Figure 11. In Figure 10, S-CTM fails to reproduce platoon dispersion and cumulative queue due to non-uniformity at intersections 2 and 3. In Figure 11, M-CTM is able to reproduce platoon dispersion as vehicles travel along the road. Furthermore, at cells 6 and 14, M-CTM can

predict the queue at intersections 2 and 3, which corresponds with control delay and queue delay from CORSIM in Table 3.

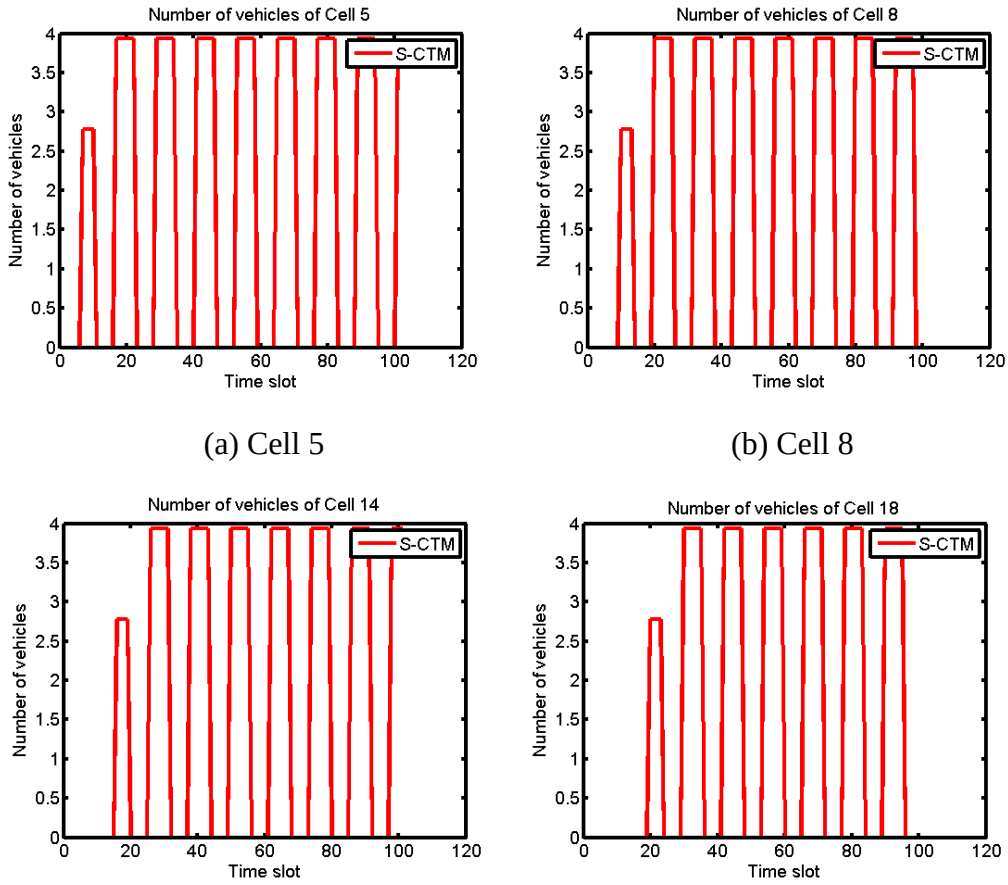

(a) Cell 5 (b) Cell 8

(c) Cell 14 (d) Cell 18

Figure 10. Number of vehicles of S-CTM after signal optimization.

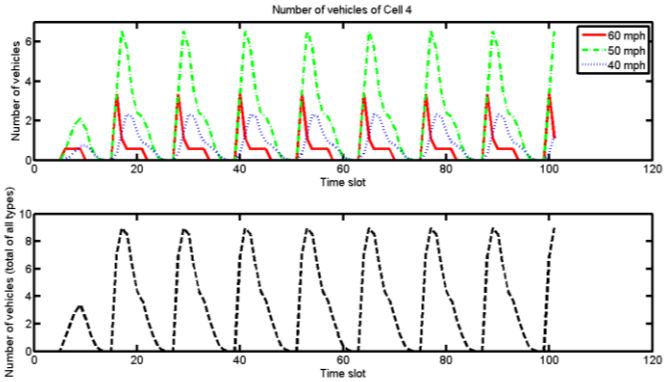

(a) Cell 4

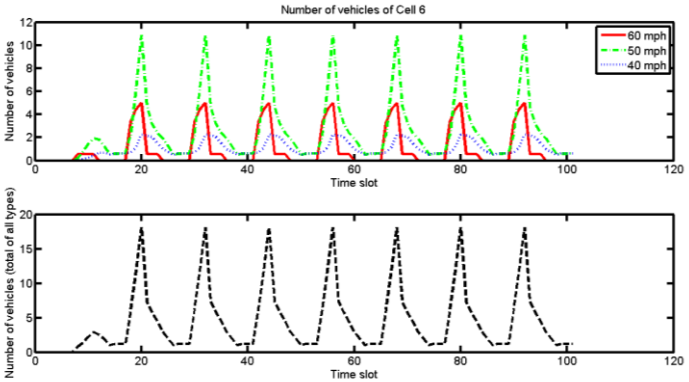

(b) Cell 6

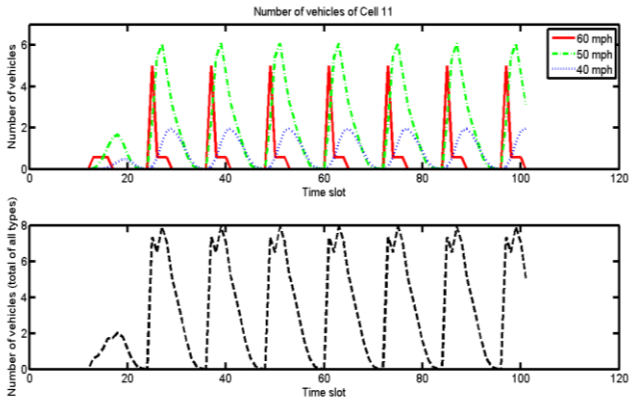

(c) Cell 11

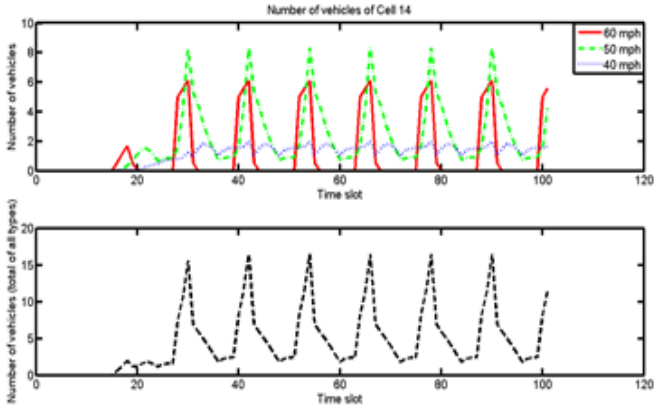

(d) Cell 14

Figure 11. Number of vehicles of M-CTM after optimizing offset.

Case 2: Non-symmetry Composition

In this case, there are three types of 16.5-foot-long vehicles with three different free-flow speeds (60, 50, and 40 mph) with a proportion equaling 0.2, 0.1, and 0.7, respectively. The calibration and signal optimization process is the same as in case 1. The calibrated parameters for S-CTM and M-CTM are shown in Table 4 and Table 5. The total delay is minimized to obtain the optimal offset for both S-CTM and M-CTM, as shown in Table 6.

Table 4. Calibrated parameters for S-CTM.

Calibrated Parameters	Lower Bound	Upper Bound	Value after Calibration
Maximum flow rate per lane per time slot	0.23	4.6	2.587
Wave propagation ratio	0.3	1	0.71
Offset for all intersections (time slot)	0	11	0

Table 5. Calibrated parameters for M-CTM.

Calibrated Parameters	Lower Bound	Upper Bound	Value after Calibration
Maximum flow rate per lane per time slot	0.23	4.6	4.554
Wave propagation ratio	0.3	1	0.84
Offsets for all intersections (time slot)	0	11	3
Normalized free-flow speed of vehicle type 2	0.5	1	0.62
Normalized free-flow speed of vehicle type 3	0.5	1	0.58

Table 6. Optimal offsets and delay from CORSIM.

	S-CTM's Offset	M-CTM's Offset
Optimal offset of intersection 1 (second)	0	0
Optimal offset of intersection 2 (second)	40	40
Optimal offset of intersection 3 (second)	30	35
Delay person-minute at intersection 2	34.5	34.9
Control delay at intersection 2 (seconds/vehicle)	0.9	0.9
Queue delay at intersection 2 (seconds/vehicle)	0.7	0.7
Stop time (seconds/vehicle)	0.7	0.7
Delay person-minute at intersection 3	35.6	30.2
Control delay at intersection 2 (seconds/vehicle)	2.3	1.4
Queue delay at intersection 2 (seconds/vehicle)	2.0	1.0
Stop time (seconds/vehicle)	1.9	0.9
Vehicle-hour of delay time	0.93	0.86

Unlike in case 1, S-CTM and M-CTM give different optimal offsets. In Table 6, S-CTM still gives the same offset as the bandwidth progression theory, whereas M-CTM gives a green time at intersection 3 sooner. Because M-CTM can predict the arrival of faster-than-average vehicles, it gives green time sooner to let these vehicles move without being stopped. On the other hand, S-CTM fails to recognize the difference in free-flow speed distribution of case 1 and case 2 and platoon dispersion, so the optimal offsets from S-CTM in both cases are the same.

Examples of S-CTM and M-CTM's density after offset optimization are shown in Figure 12 and Figure 13. In Figure 12, S-CTM fails to reproduce platoon dispersion. In Figure 13, M-CTM is able to reproduce platoon dispersion as vehicles travel along the road.

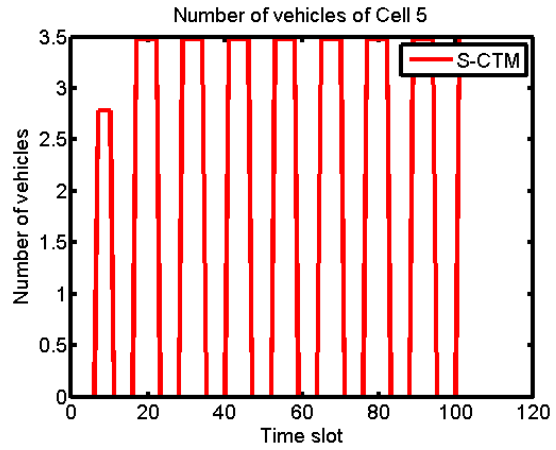

(a) Cell 5

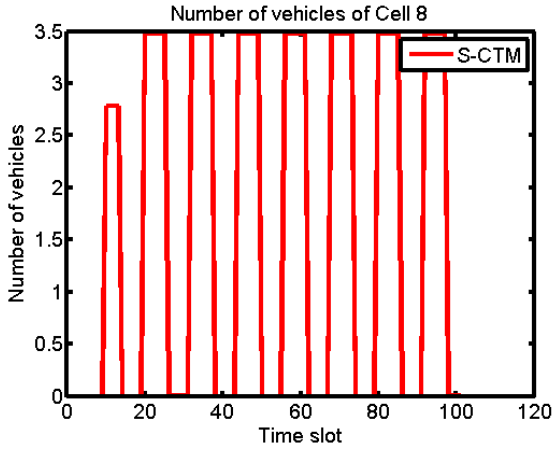

(b) Cell 8

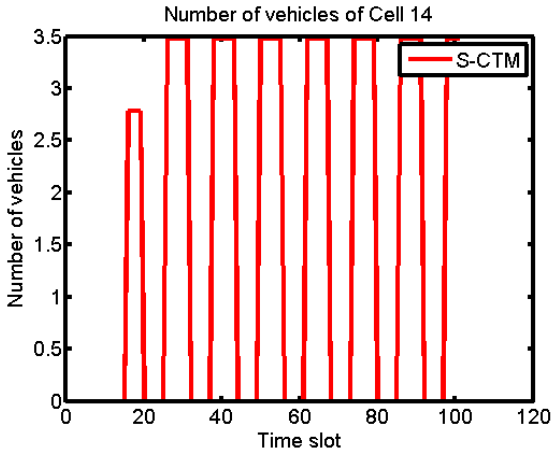

(c) Cell 14

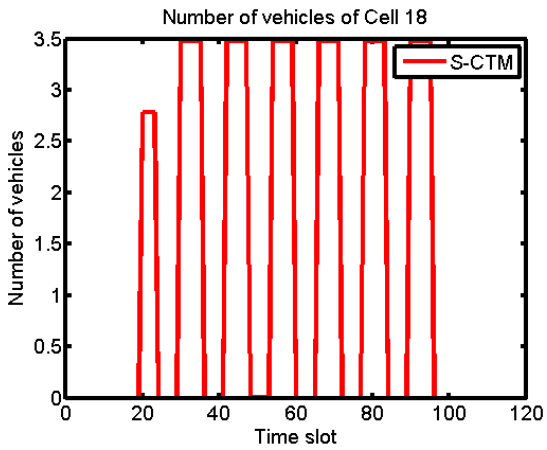

(d) Cell 18

Figure 12. Number of vehicles of S-CTM after signal optimization.

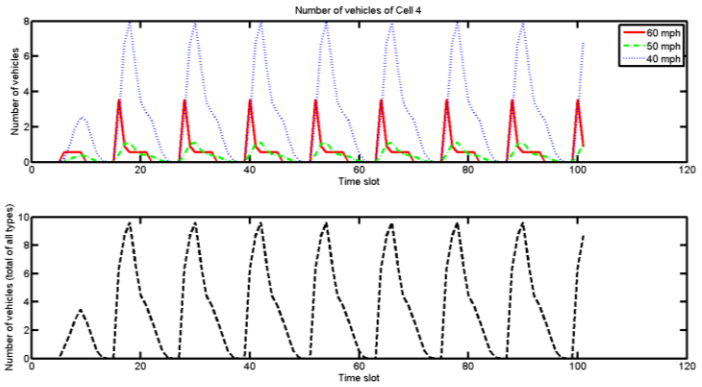

(a) Cell 4

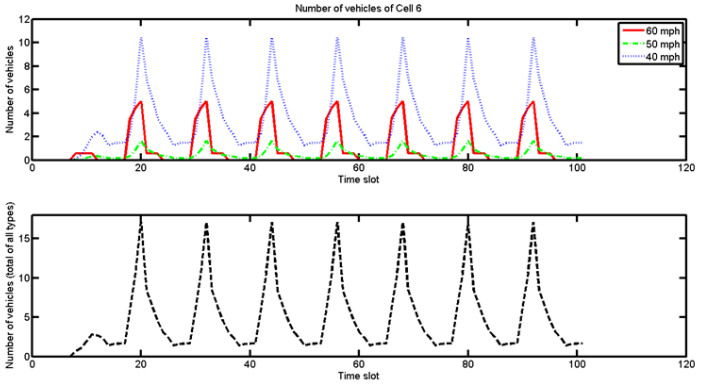

(b) Cell 6

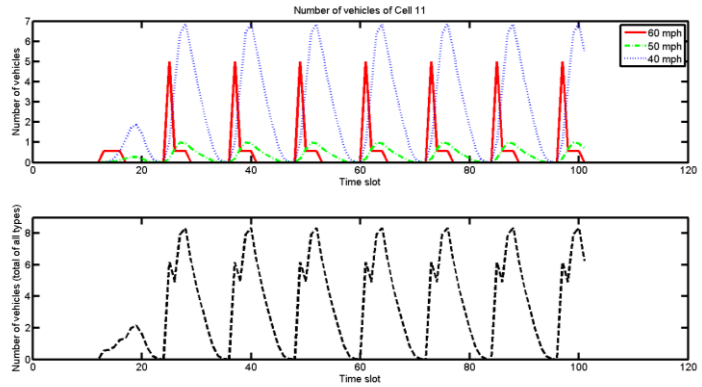

(c) Cell 11

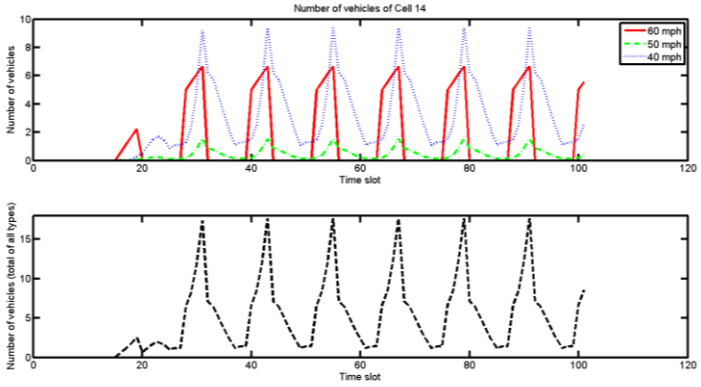

(d) Cell 14

Figure 13. Number of vehicles of M-CTM after optimizing offset.

NUMERICAL RESULTS FOR QUEUE LENGTH ESTIMATION USING CV DATA

To test queue length estimation from CV data, microscopic simulation, VISSIM, was selected as a test bed to generate individual vehicles' information and observe queue length. The necessary individual vehicle data from VISSIM are instantaneous speed and distance from the approaching intersection. The queue lengths from the proposed algorithm are compared with the queue length obtained directly from VISSIM.

To demonstrate a penetration ratio, part of the individual data is randomly removed from queue length estimation corresponding to the penetration ratio. For example, if the ratio is 30 percent, 30 percent of each individual vehicle's data is used in the estimation. The greater the penetration ratio, the more data are missing. To nullify the effect of randomness, each case is simulated 100 times, and then the root mean square error is averaged.

The test network is an isolated intersection with two lanes in each direction, as shown in Figure 14. The simulation time is 1,000 seconds. Each approach is a 882-foot-long road. The volume for each case is varied. The signal control is set to either fixed-time or actuated control depending on the case. The stopping speed is set to 0 mph. VISSIM's results show queue length in terms of average queue length as a time interval of 2 seconds. Individual vehicles' data are collected every 0.5 seconds. Therefore, queue length estimation is calculated every 0.5 seconds, and then averaged and maximized for every time interval of 2 seconds to compare with the queue length data from VISSIM. The numerical results are divided into four cases based on the type of signal control and volume used in the simulations. Since Comert's algorithm needs the duration of red time and the probability function of the actual queue in the calculation, these data are obtained from VISSIM. However, such information is rarely available in practice.

The experiments can be divided into four cases:

- Fixed signal control.
- Actuated signal control.
- Undersaturated conditions.
- Saturated conditions.

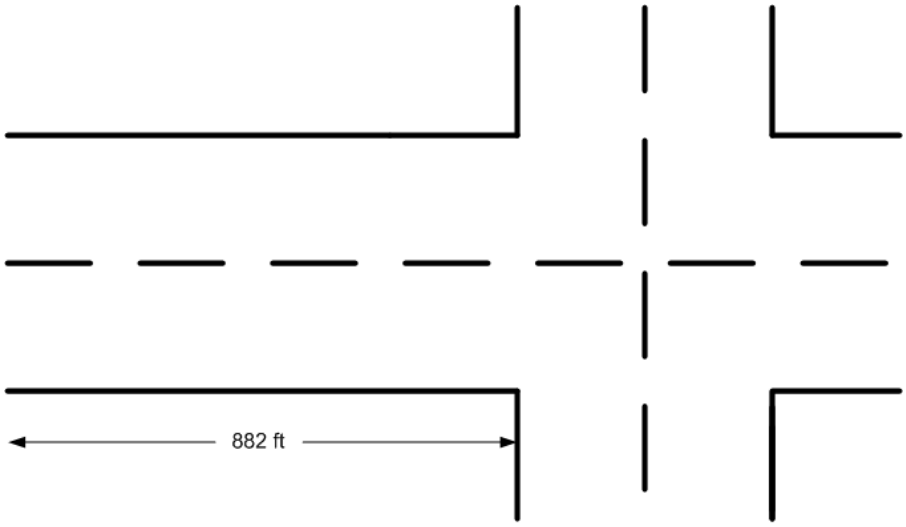

Figure 14. Isolated intersection used in queue length estimation.

In fixed signal cases, the comparisons between the proposed algorithm and Comert's algorithm are given. However, since Comert's algorithm is applicable only with fixed signals, only numerical results for the proposed algorithm are given in the cases of actuated control.

Case 1: Fixed Signal Control with Undersaturated Condition

In this case, the signal control is set to be pre-timed with green and red time to be 30 seconds. The volume for two lanes is 1,000 vph with a Poisson arrival rate.

Figure 15 through Figure 20 show the results of queue length estimation for the proposed algorithm and Comert's algorithm for a penetration ratio equaling 30, 50, and 80 percent, respectively.

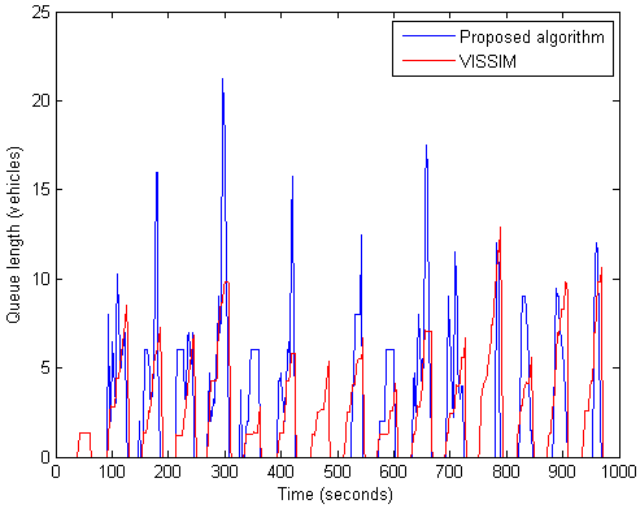

Figure 15. Estimated queue length of proposed algorithm when penetration ratio is 30 percent.

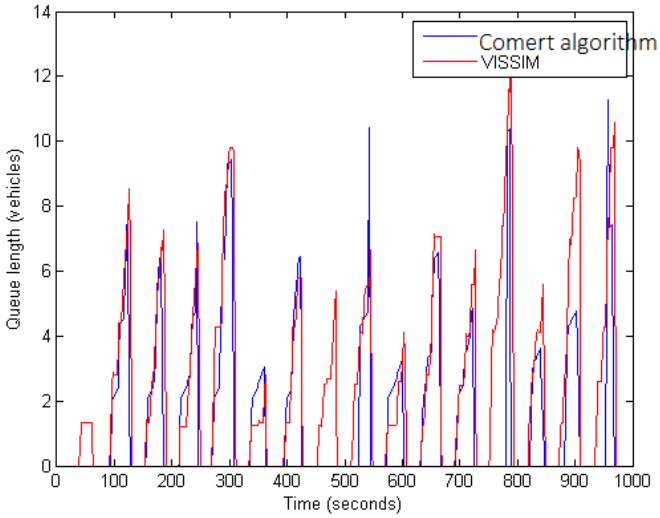

Figure 16. Estimated queue length of Comert's algorithm when penetration ratio is 30 percent.

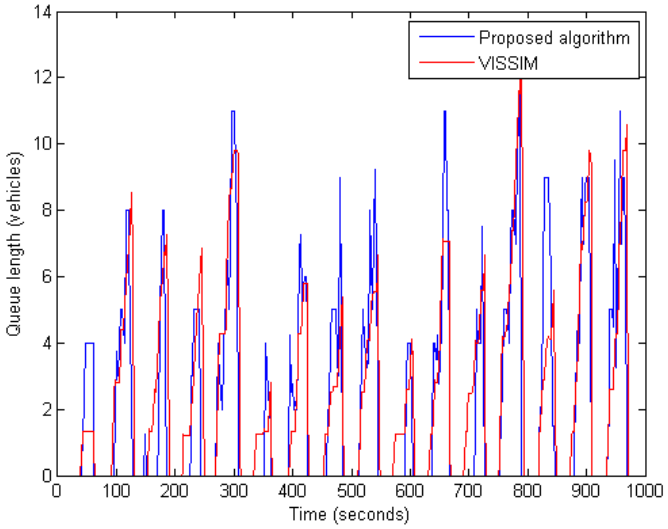

Figure 17. Estimated queue length of proposed algorithm when penetration ratio is 50 percent.

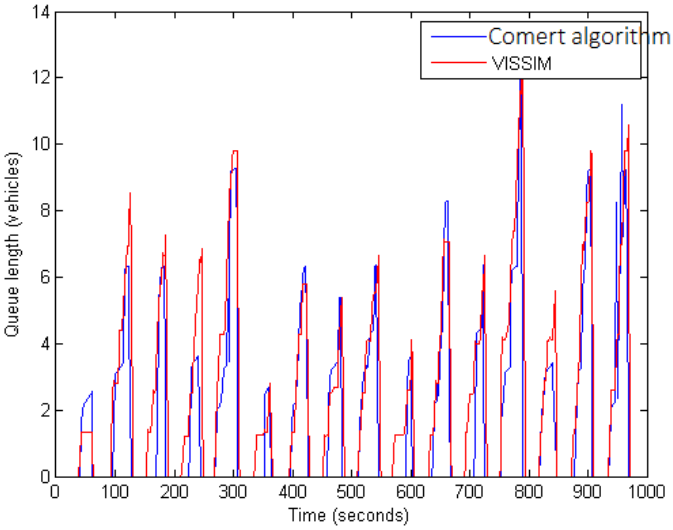

Figure 18. Estimated queue length of Comert's algorithm when penetration ratio is 50 percent.

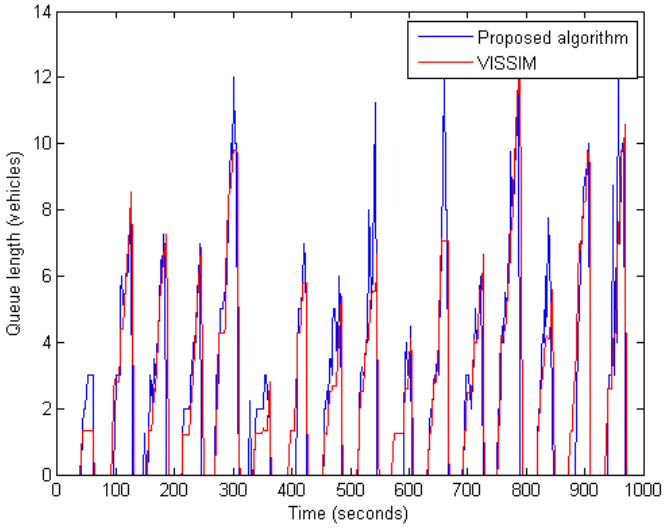

Figure 19. Estimated queue length of proposed algorithm when penetration ratio is 80 percent.

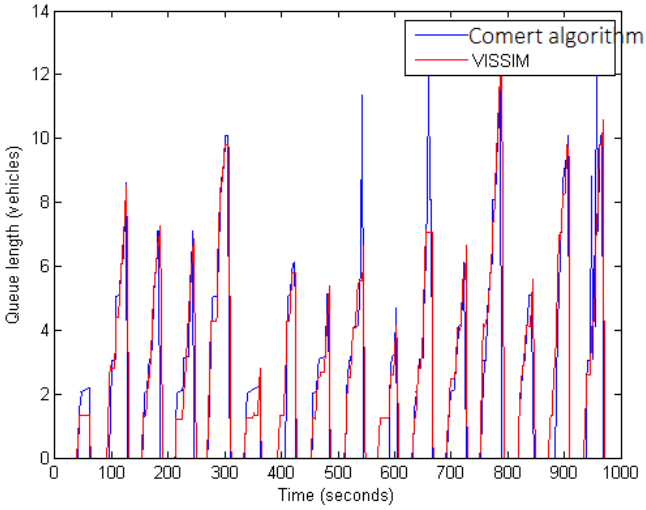

Figure 20. Estimated queue length of Comert's algorithm when penetration ratio is 80 percent.

Case 2: Fixed Signal Control with Saturated Condition

In this case, the signal control is the same as in case 1, but the volume is set to 1,400 vph. The Poisson arrival assumption is not valid in this case since traffic is not in the undersaturated condition.

Figure 21 through Figure 26 show the results of queue length estimation for a penetration ratio equal to 30, 50, and 80 percent, respectively.

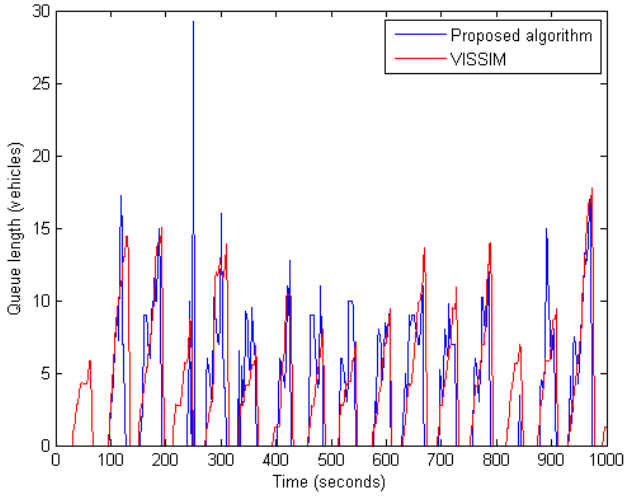

Figure 21. Estimated queue length of proposed algorithm when penetration ratio is 30 percent.

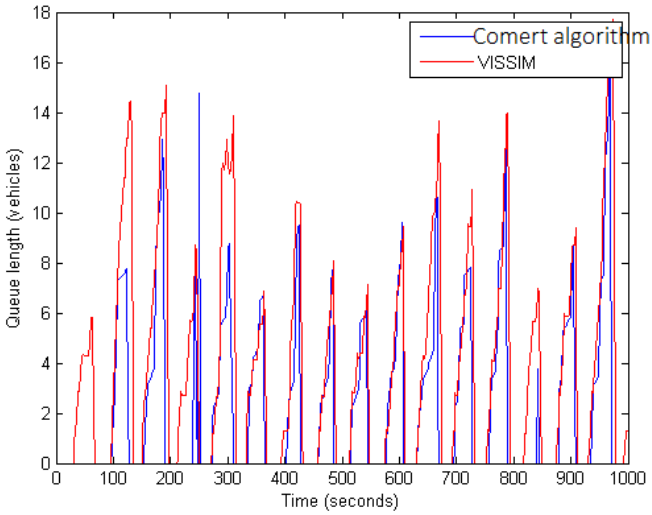

Figure 22. Estimated queue length of Comert's algorithm when penetration ratio is 30 percent.

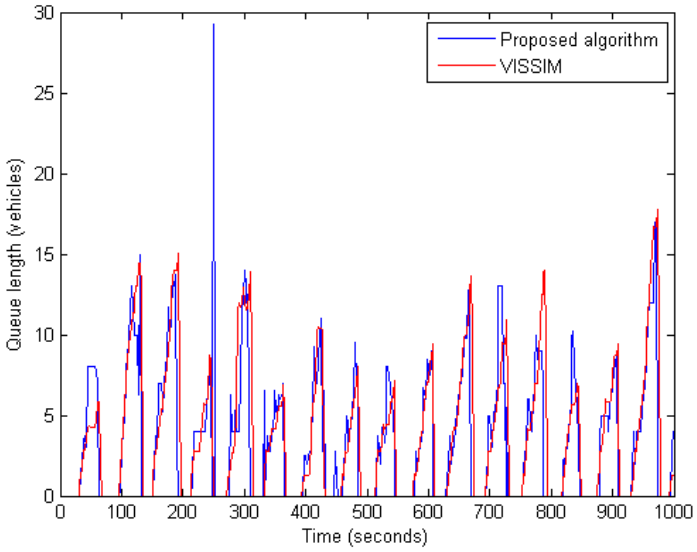

Figure 23. Estimated queue length of proposed algorithm when penetration ratio is 50 percent.

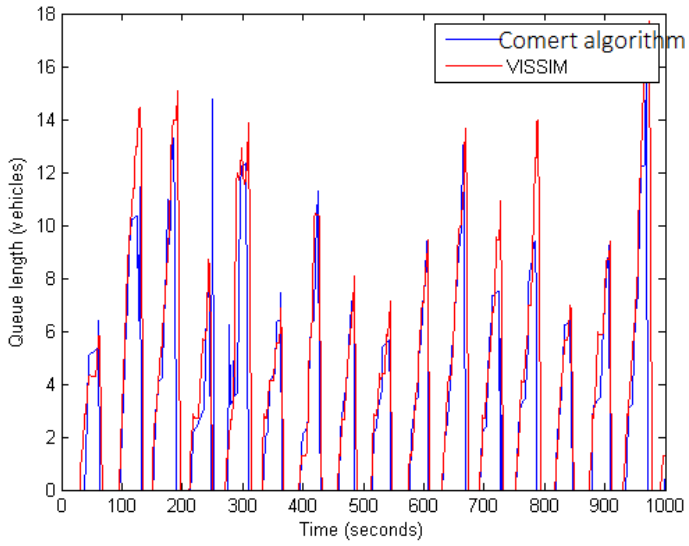

Figure 24. Estimated queue length of Comert's algorithm when penetration ratio is 50 percent.

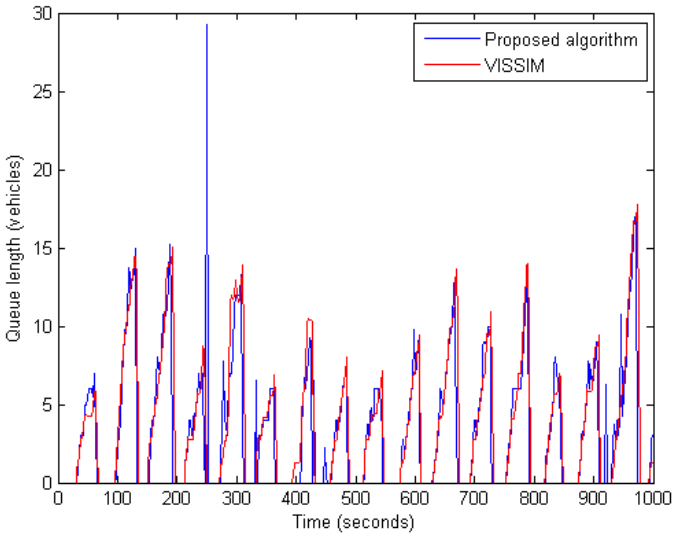

Figure 25. Estimated queue length of proposed algorithm when penetration ratio is 80 percent.

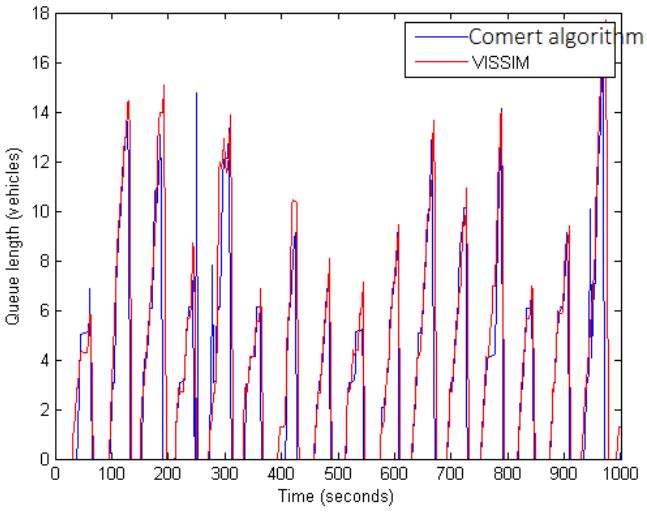

Figure 26. Estimated queue length of Comert's algorithm when penetration ratio is 80 percent.

Case 3: Actuated Signal Control with Undersaturated Condition

In this case, the signal control is set to actuated control with the undersaturated condition. Only numerical results of the proposed algorithm are given. The traffic volume is set to 1,000 vph.

Figure 27 through Figure 29 show the results of queue length estimation for a penetration ratio equaling 30, 50, and 80 percent, respectively.

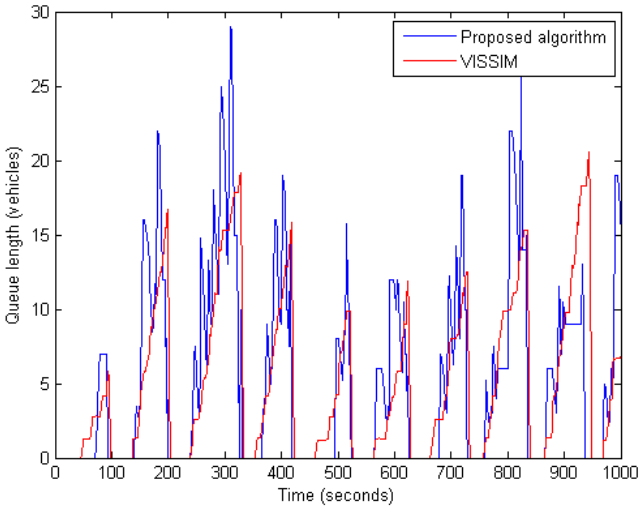

Figure 27. Estimated queue length of proposed algorithm when penetration ratio is 30 percent.

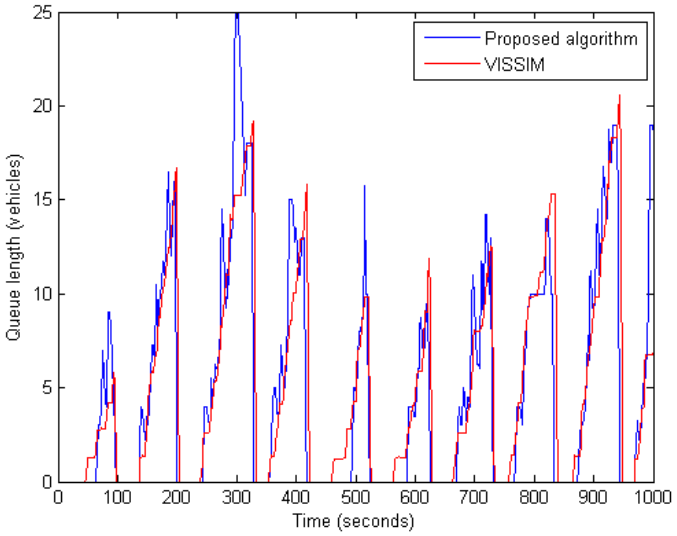

Figure 28. Estimated queue length of proposed algorithm when penetration ratio is 50 percent.

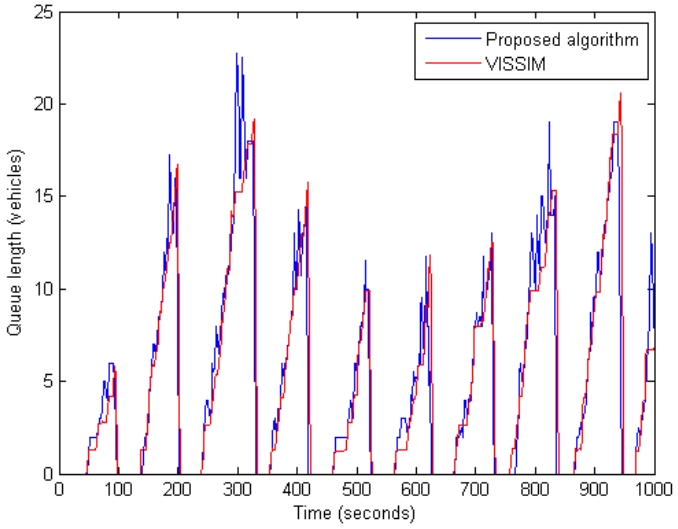

Figure 29. Estimated queue length of proposed algorithm when penetration ratio is 80 percent.

Case 4: Actuated Signal Control with Saturated Condition

This case is similar to case 3, but the traffic volume is set to 1,400 vph. Figure 30 through Figure 32 show the results of queue length estimation for a penetration ratio equaling 30, 50, and 80 percent, respectively.

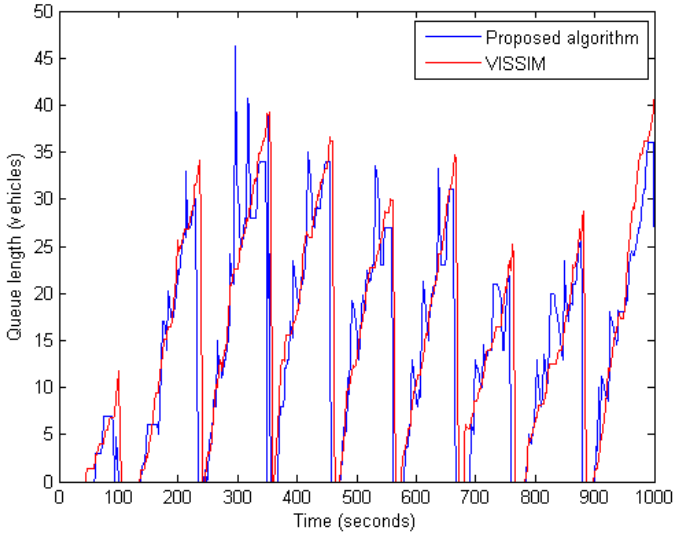

Figure 30. Estimated queue length of proposed algorithm when penetration ratio is 30 percent.

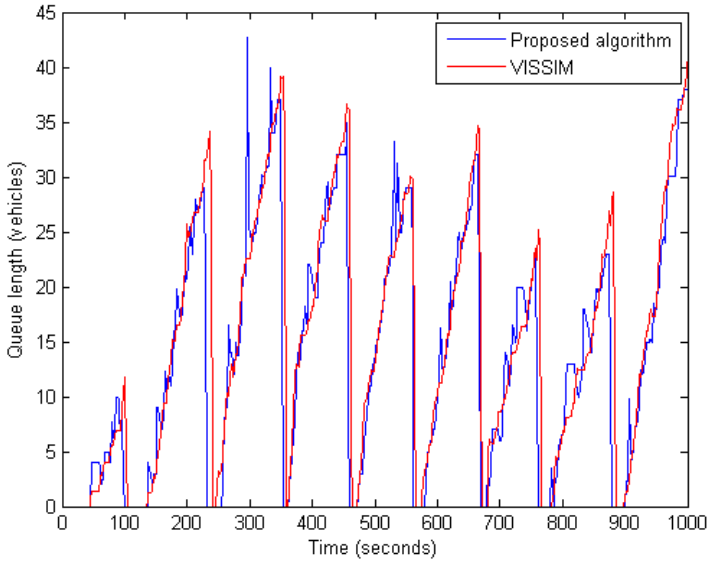

Figure 31. Estimated queue length of proposed algorithm when penetration ratio is 50 percent.

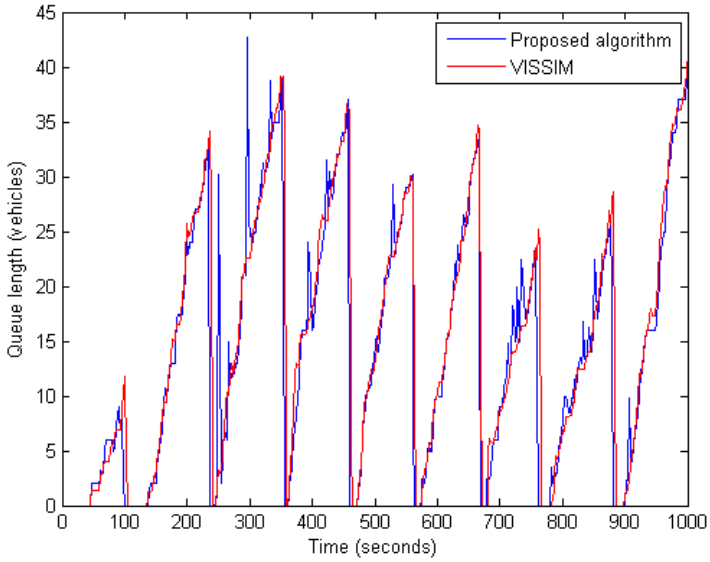

Figure 32. Estimated queue length of proposed algorithm when penetration ratio is 80 percent.

The Proposed Algorithm with Wavelet Transform

This section demonstrates the numerical results after applying discrete wavelet transform (DWT) to all four cases. Wavelet transform is a powerful tool used to filter out unwanted noise

or error with multi-resolution properties [40, 41]. The time series of queue length estimation is filtered out through high-pass and low-pass filters to obtain approximation and detailed components. The detailed component is assumed to be mostly noise since queue forming and dissipation are rather slow compared to such an unwanted random spikes in the graph. As a result, only an approximation component is used to represent the queue length. Even though this assumption might be too simplistic and a soft or hard threshold should be used instead, this research project is the first to demonstrate DWT and prove its merit for queue length estimation. Moreover, to apply a threshold scheme, the characteristics of the error of queue length estimation and the actual queue length in the frequency domain must be understood. This issue is out of the scope of this research project but is worthy of future research nonetheless.

Figure 33 through Figure 44 show the estimated queue length of the proposed algorithm when penetration is 30 percent after applying wavelet transform level 1–3.

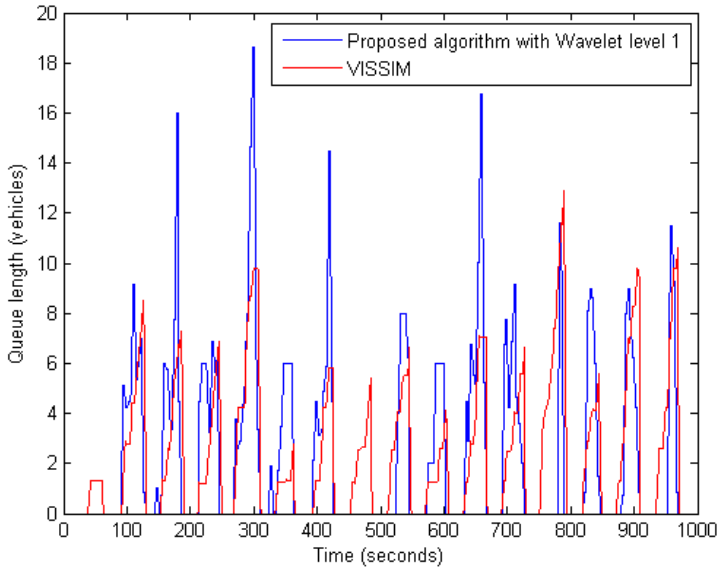

Figure 33. Wavelet transform level 1 of estimated queue length in case 1: fixed signal control with undersaturated condition.

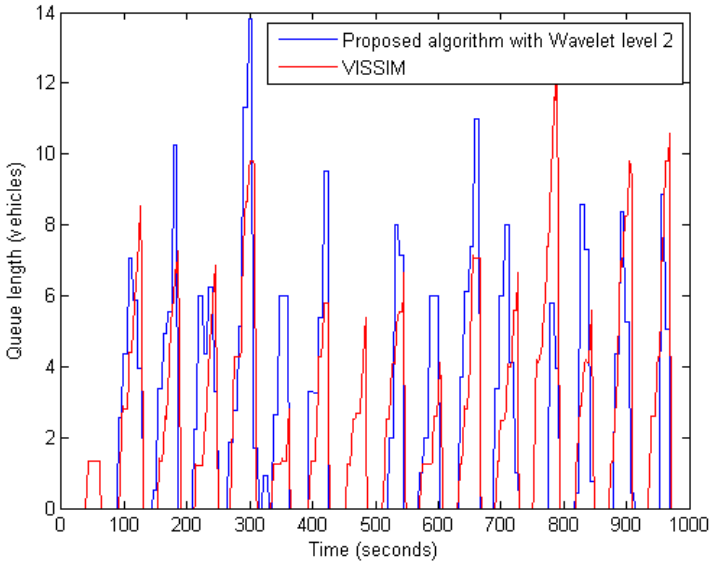

Figure 34. Wavelet transform level 2 of estimated queue length in case 1: fixed signal control with undersaturated condition.

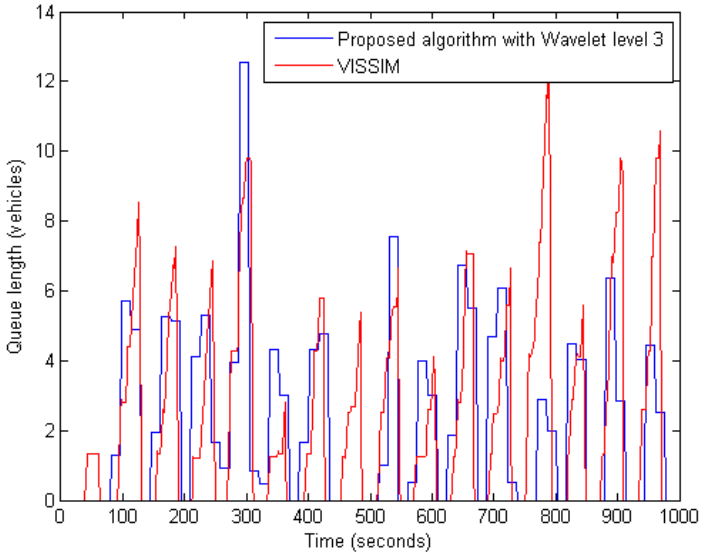

Figure 35. Wavelet transform level 3 of estimated queue length in case 1: fixed signal control with undersaturated condition.

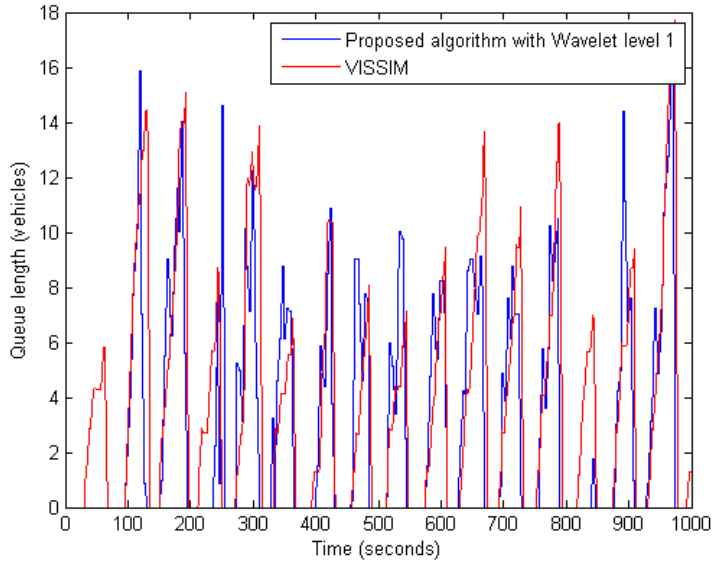

Figure 36. Wavelet transform level 1 of estimated queue length in case 2: fixed signal control with saturated condition.

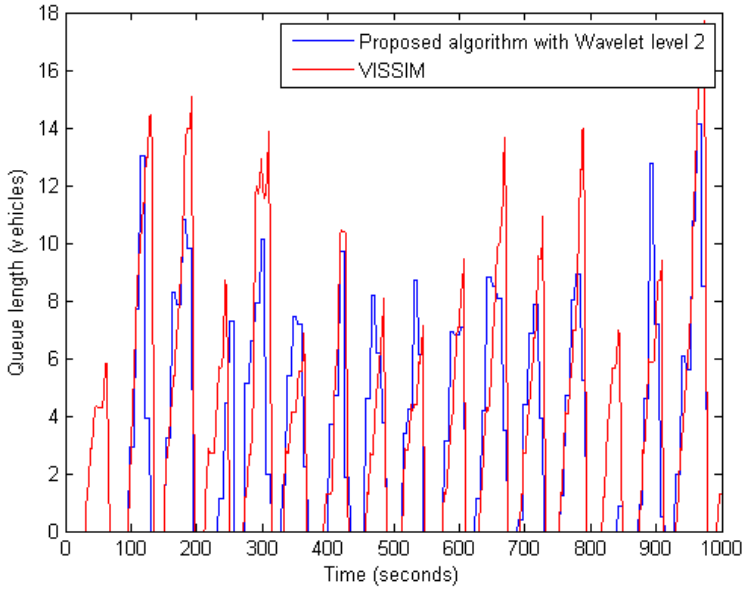

Figure 37. Wavelet transform level 2 of estimated queue length in case 2: fixed signal control with saturated condition.

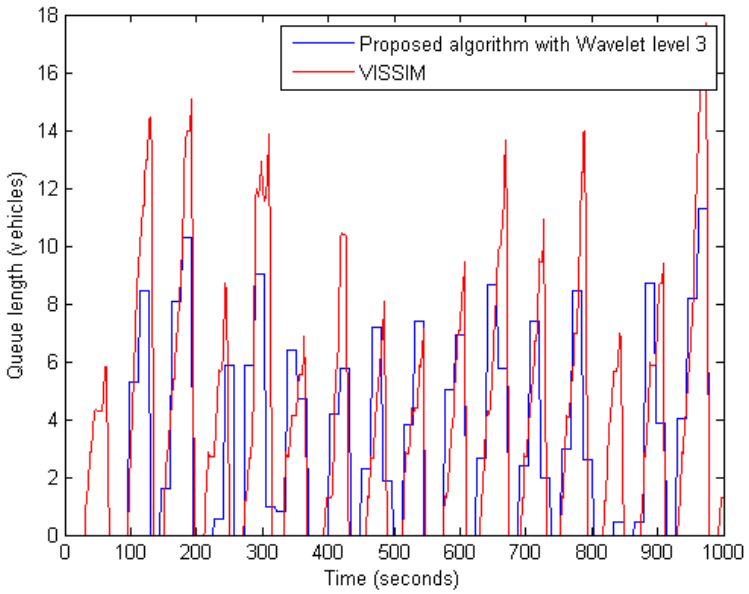

Figure 38. Wavelet transform level 3 of estimated queue length in case 2: fixed signal control with saturated condition.

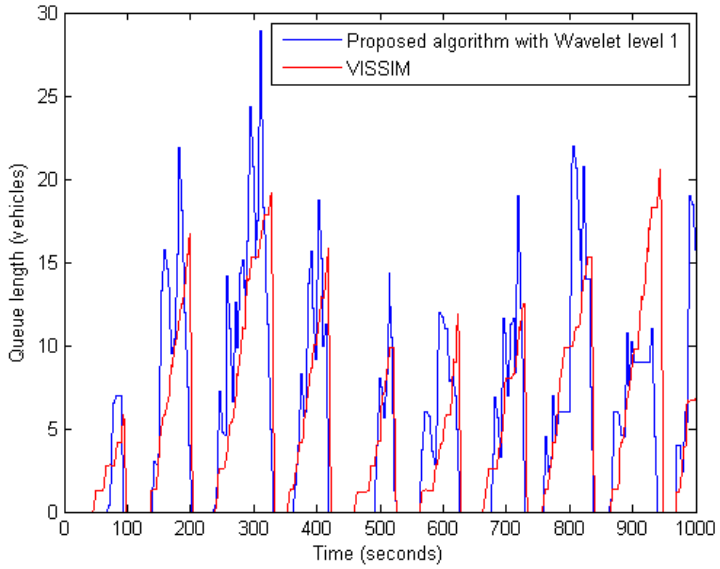

Figure 39. Wavelet transform level 1 of estimated queue length in case 3: actuated signal control with undersaturated condition.

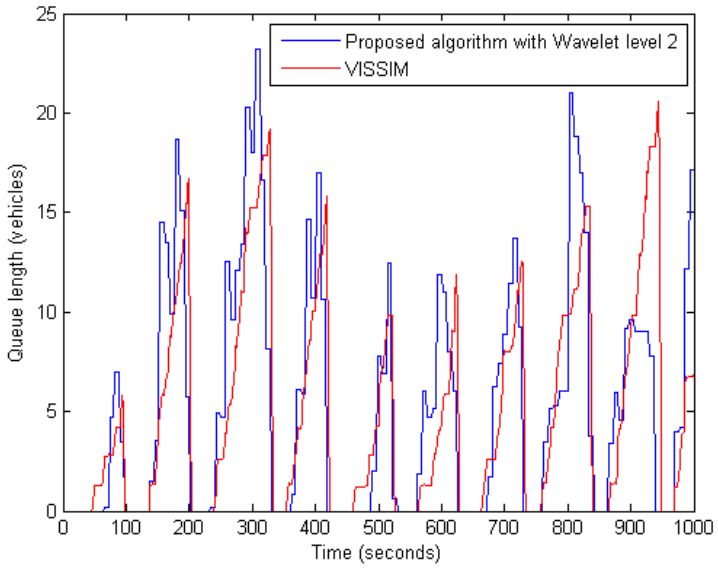

Figure 40. Wavelet transform level 2 of estimated queue length in case 3: actuated signal control with undersaturated condition.

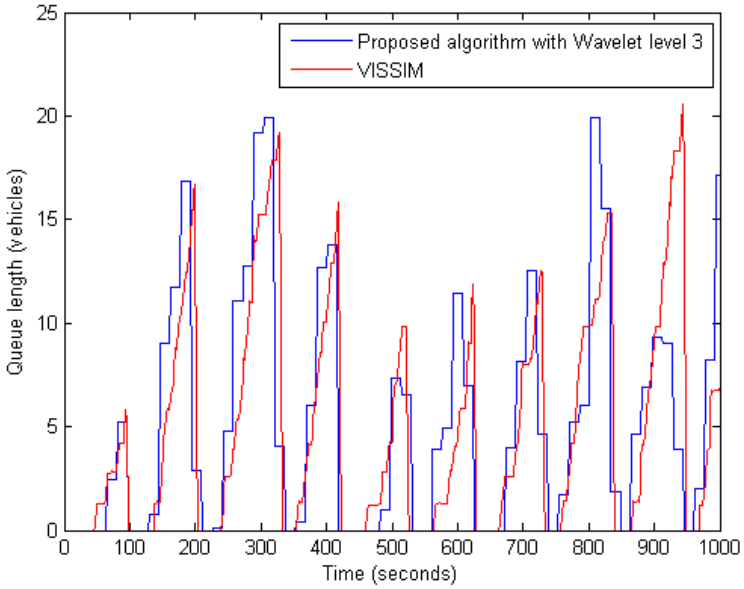

Figure 41. Wavelet transform level 3 of estimated queue length in case 3: actuated signal control with undersaturated condition.

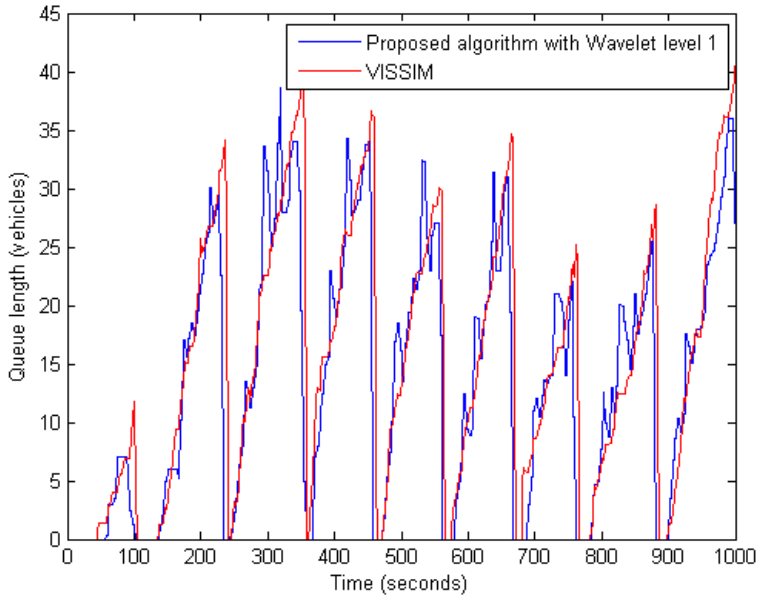

Figure 42. Wavelet transform level 1 of estimated queue length in case 4: actuated signal control with saturated condition.

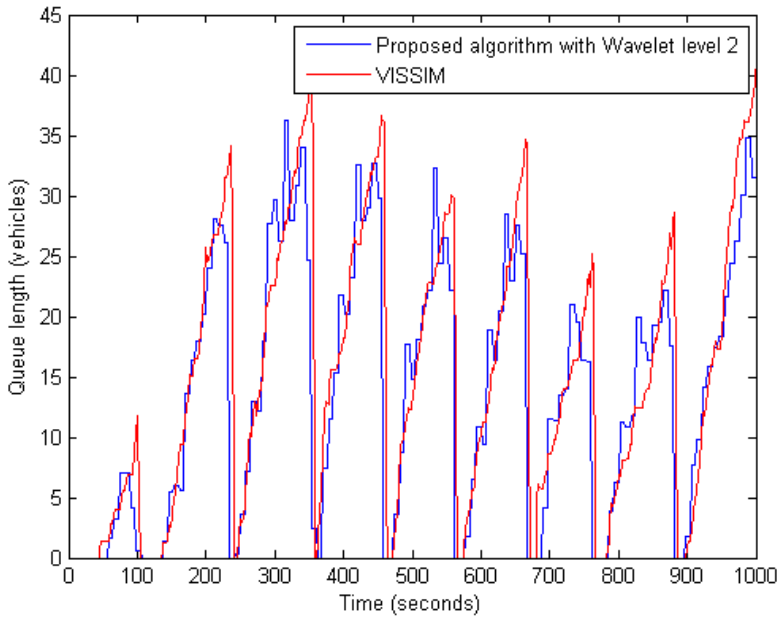

Figure 43. Wavelet transform level 2 of estimated queue length in case 4: actuated signal control with saturated condition.

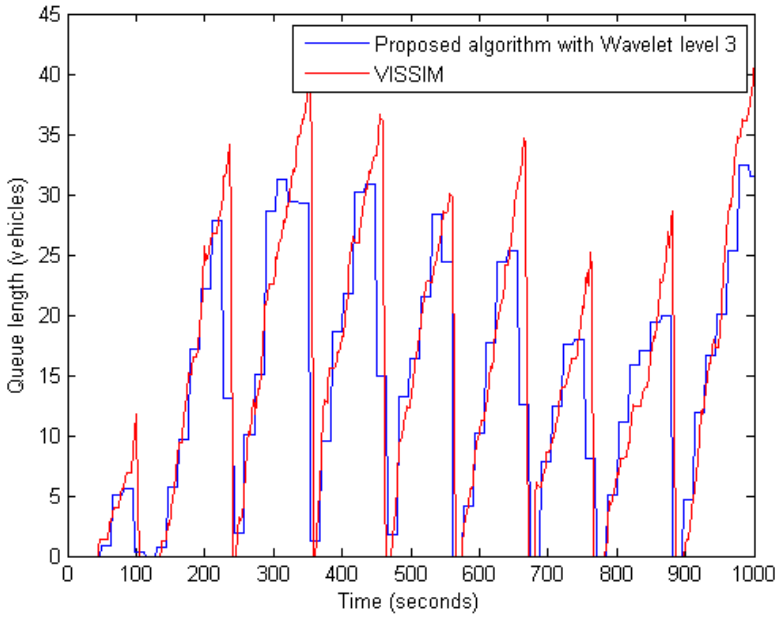

Figure 44. Wavelet transform level 3 of estimated queue length in case 4: actuated signal control with saturated condition.

The root mean square error versus penetration of four cases is shown in Figure 45 through Figure 48.

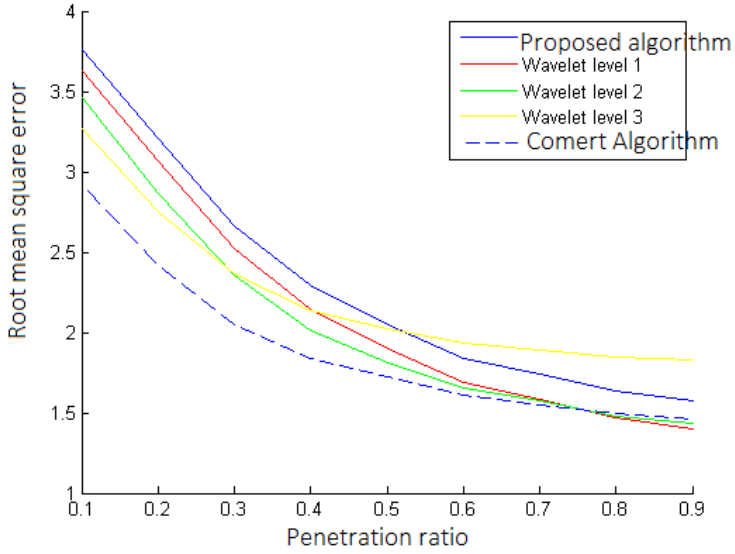

Figure 45. Root mean square error of queue length estimation in case 1: fixed signal control with undersaturated condition

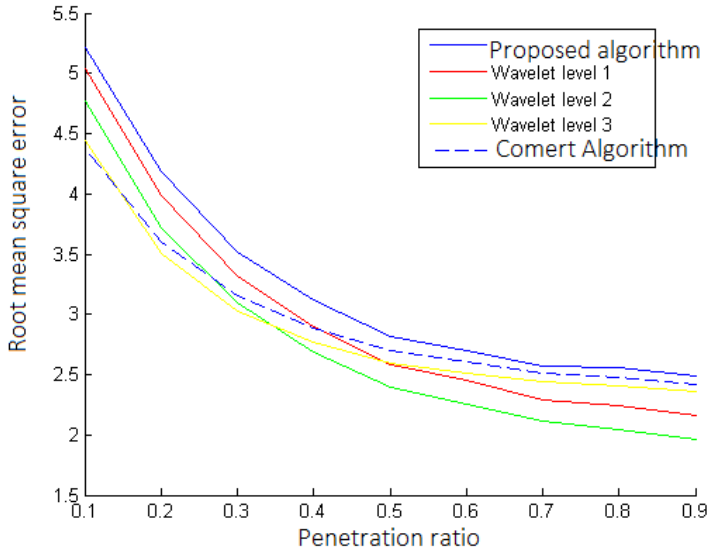

Figure 46. Root mean square error of queue length estimation in case 2: fixed signal control with saturated condition.

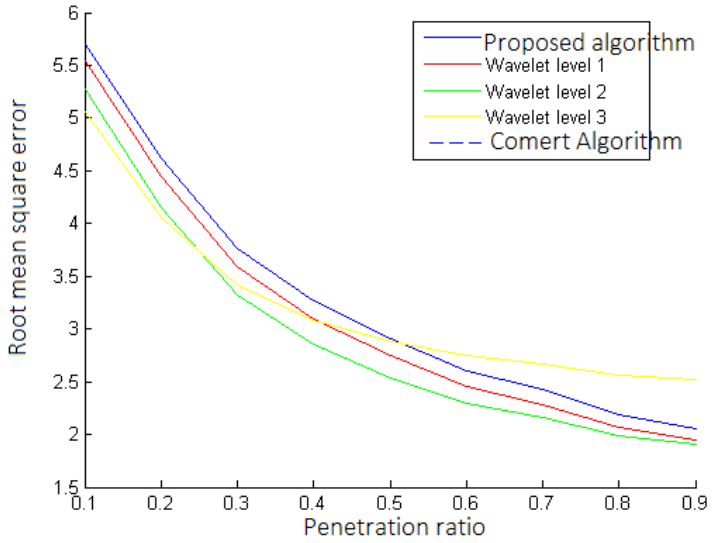

Figure 47. Root mean square error of queue length estimation in case 3: actuated signal control with undersaturated condition.

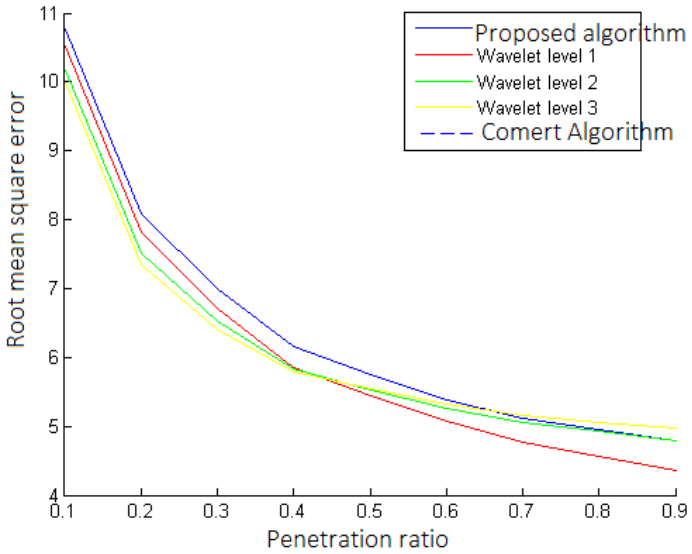

Figure 48. Root mean square error of queue length estimation in case 4: actuated signal control with saturated condition.

DWT can improve queue length estimation—not only RMSE but its consistency. Unwanted error spikes are eliminated after DWT is applied to the time series of queue length estimation. Removal of random spikes is essential for adaptive signal control since the random spikes can be misleading and put the optimized signal far from the actual optimal signal. As shown by Figure 45 through Figure 48, DWT does decrease RMSE. The different levels of DWT work best at the different ranges of penetration ratio. Low-level DWT works best at a high penetration ratio since it retains a dynamic-capture part. High-level DWT eliminate most of the detailed component, which, in turn, disables the ability to track a dynamic change in the actual queue length. On the other hand, high-level DWT performs best at a low penetration ratio since most detailed components are estimation errors that need to be removed. Low-level DWT cannot filter out noise as well as high-level DWT in this case.

NUMERICAL RESULTS FOR ADAPTIVE SIGNAL CONTROL LOGIC

The test network is a road network composed of two intersections with four lanes in each direction, as shown in Figure 49. The simulation time is 1,800 seconds. The volume for each approach is varied from case to case. Free-flow speed is 60 feet per second. The maximum flow

rate is 0.59 vehicles per second per lane. There is only through movement with a two-phase signal plan. The lost time when the traffic light turns from red to green is 2 seconds.

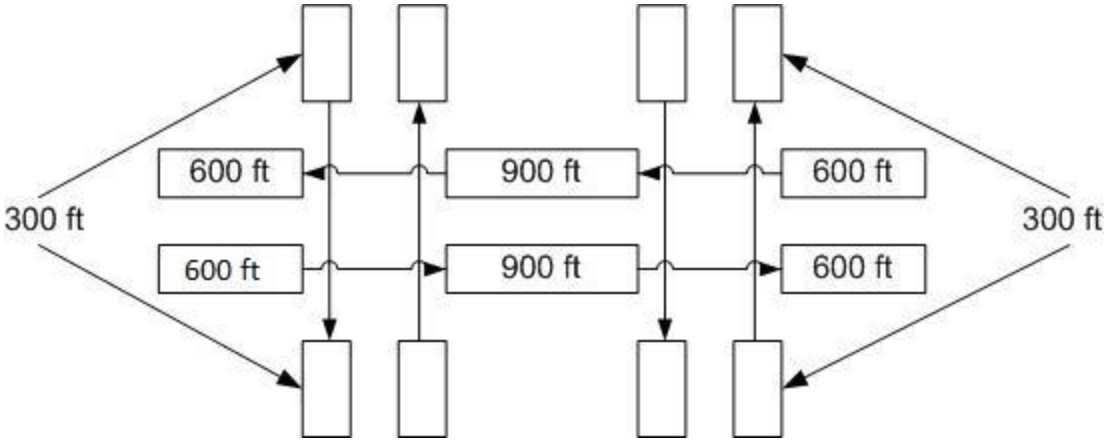

Figure 49. Test network for adaptive signal control logic.

The adaptive signal control logic was tested on a macroscopic simulation, single-class cell transmission model. The vehicle's length is 15 feet. The time interval is 1 second, and the total time interval is 1,800 seconds. The tests are divided into two cases based on the type of arrival:

- Constant arrival.
- Platoon arrival.

A penetration ratio is assumed to be 100 percent. In other word, all vehicles and their distance and queue lengths from S-CTM are known and input into adaptive signal control to determine a signal plan for each time.

Case 1: Constant Arrival

In this case, the incoming vehicle to the road network is constant over time. This case is divided into two subcases: the free-flow condition and the congestion condition. The free-flow condition has the input 4,000 vph for all approaches, and the congestion condition has 2,000 vph. The results are shown in Table 7 and Table 8.

Table 7. Optimal delay and signal plans from case 1 with free-flow condition.

	Optimal Pre-timed Plan	Adaptive Signal Plan
Total delay	5.85 seconds	5.85 seconds
Signal plan for intersection 1	10/10	10/10
Signal plan for intersection 2	10/10	10/10

Table 8. Optimal delay and signal plans from case 1 with congestion condition.

	Optimal Pre-timed Plan	Adaptive Signal Plan
Total delay	146 seconds	146 seconds
Signal plan for intersection 1	63/69	See Figure 50-51
Signal plan for intersection 2	21/20	See Figure 52-53

Green time for intersection 1 and 2 are not constant and vary with time. Green time of intersection 1 and 2 are shown in Figure 50 through Figure 55.

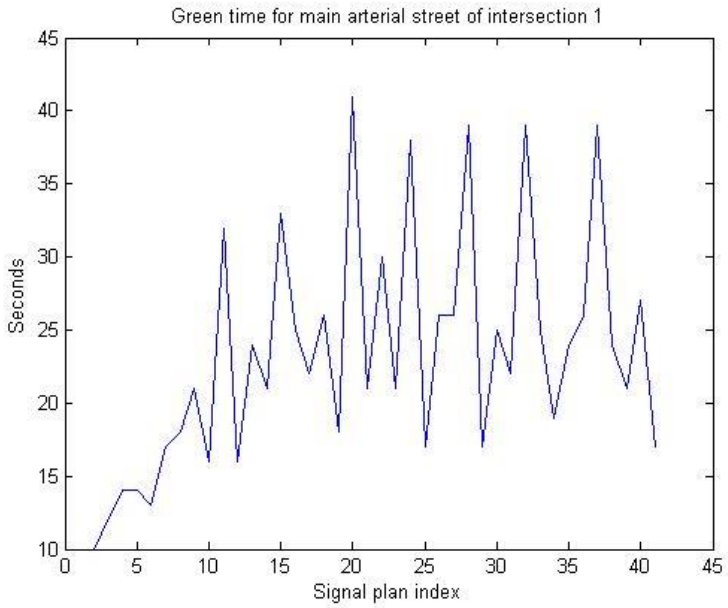

Figure 50. Green time for main arterial road of intersection 1 in congestion condition.

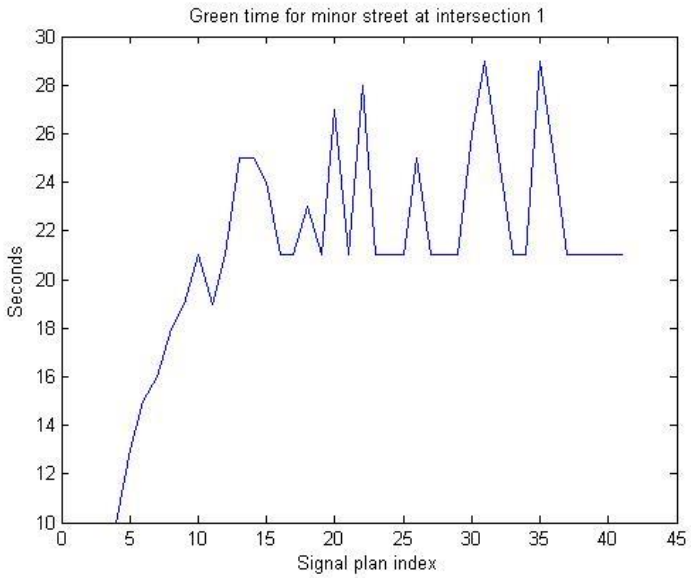

Figure 51. Green time for minor road of intersection 1 in congestion condition.

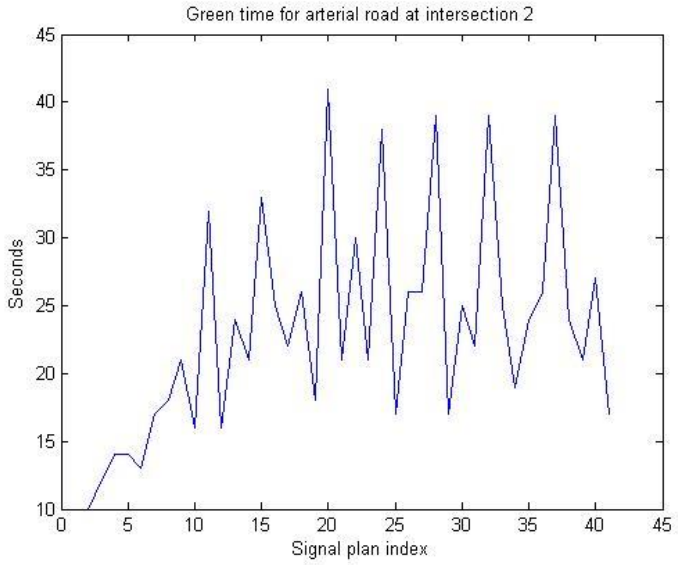

Figure 52. Green time for main arterial road of intersection 2 in congestion condition.

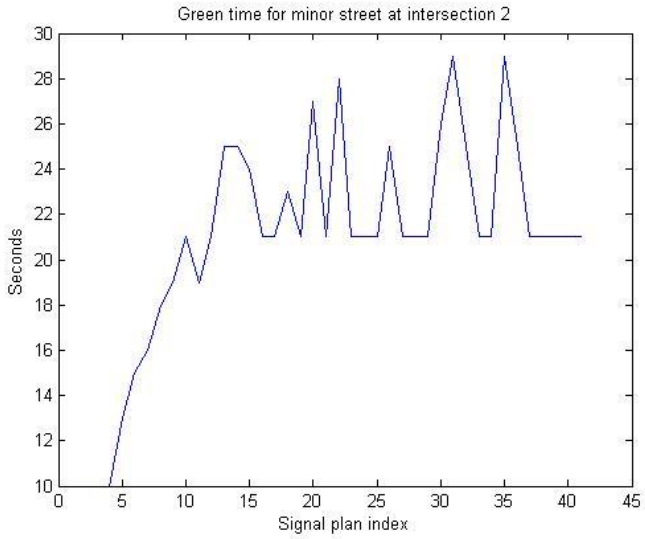

Figure 53. Green time for minor road of intersection 2 in congestion condition.

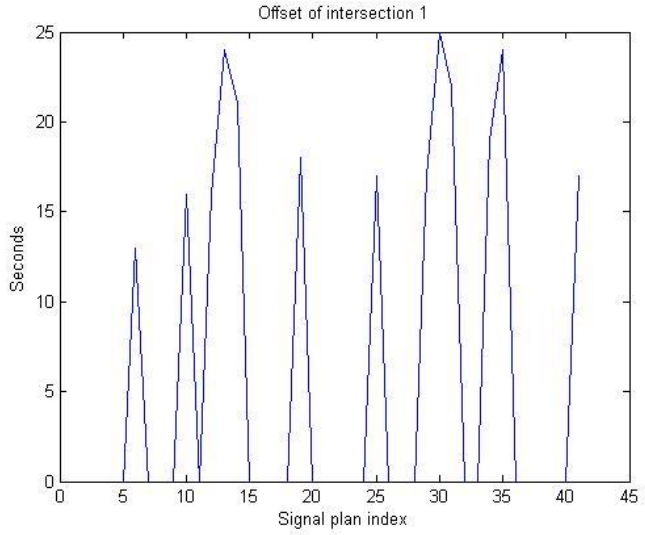

Figure 54. Offset of intersection 1 in congestion condition.

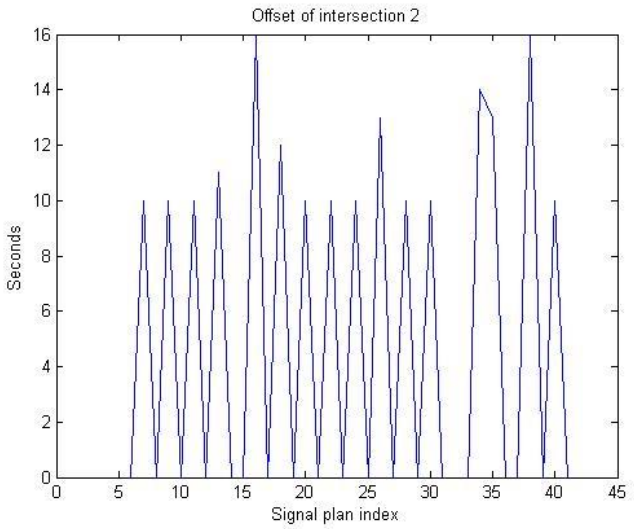

Figure 55. Offset of intersection 2 in congestion condition.

In this case, the optimal pre-timed signal plan and adaptive signal plan give the same total delay. However, signal plans are different in the congestion condition. For the congestion condition, adaptive signal control switches from the congestion mode to the coordination mode when the queue is small. Then it goes back to the congestion mode when the queue has accumulated again. Adaptive signal control cannot improve total delay in both subcases because the input is constant. The optimal pre-timed plan can find the best signal plans, and there is no space for improvement.

Case 2: Platoon Arrival

In this case, the incoming vehicle is not constant over time on all approaches but enters the system as a platoon, as shown in figure 56. For the main arterial roads, the vehicles enter the road network as a platoon. For the minor roads, the vehicles still arrive at a constant rate as in case 1. Both major and minor roads have a volume of 2,000 vph. The result is shown in Table 9.

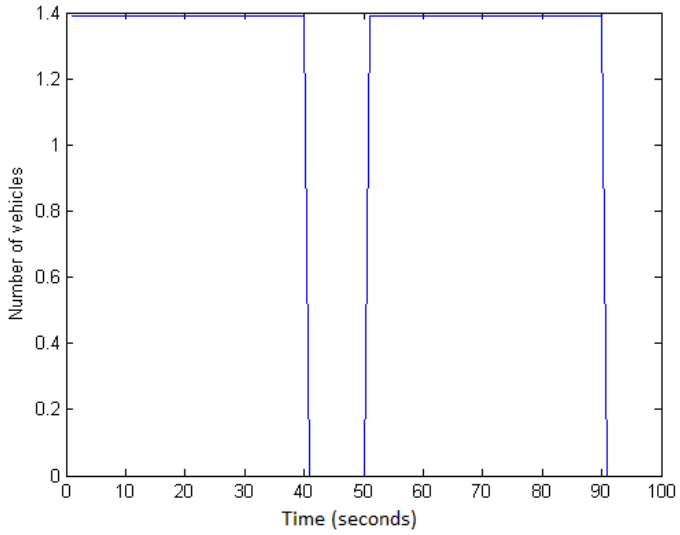

Figure 56. Platoon arrival input for case 2: platoon arrival.

Table 9. Optimal delay and signal plans from case 2.

	Optimal Pre-timed Plan	Adaptive Signal Plan
Total delay	16.35 seconds	6.75 seconds
Signal plan for intersection 1	40/19	See Figures 57-58
Signal plan for intersection 2	56/47	See Figures 59-60

In this case, adaptive signal control can give a significantly lower total delay. Comparing the result with the free-flow condition of case 1, the total volume is the same, 2,000 vph for each approach. However, the delay-optimal pre-timed plan increases from 5.85 to 16.35 seconds, and the adaptive signal plan increases just a little from 5.85 to 6.75 seconds. The distance of incoming vehicles from CV data can be of benefit in this case because it enables adaptive signal control to adjust the green time and offset based on the arrival time to the intersection. In addition, adaptive signal control does not have to waste green time for the arterial road when there is no platoon for a short time.

As shown in Figure 57 through Figure 62, unlike in case 1 with the free-flow condition, green times for the arterial road are adaptive, based on the input over time. The real benefit of adaptive signal control is when the input is not constant over time and needs a signal plan that is not fixed over time.

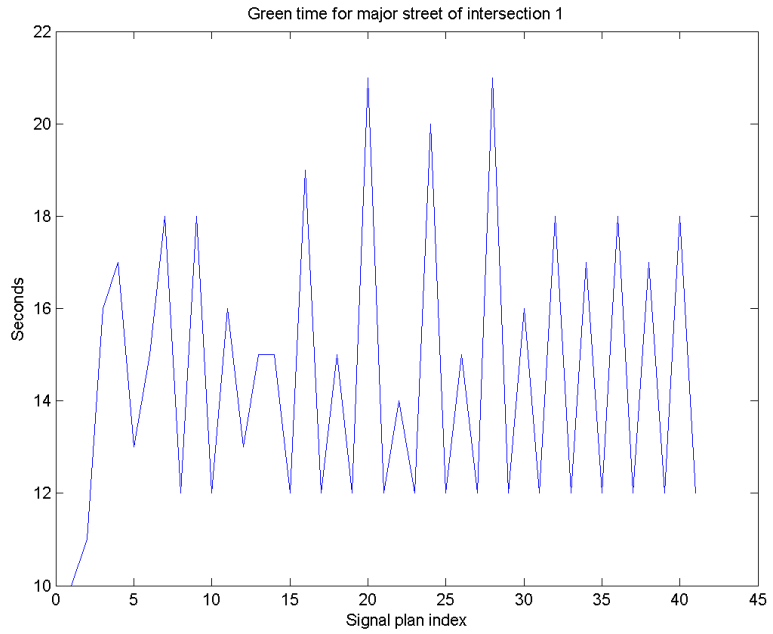

Figure 57. Green time for main arterial road of intersection 1 in platoon arrival case.

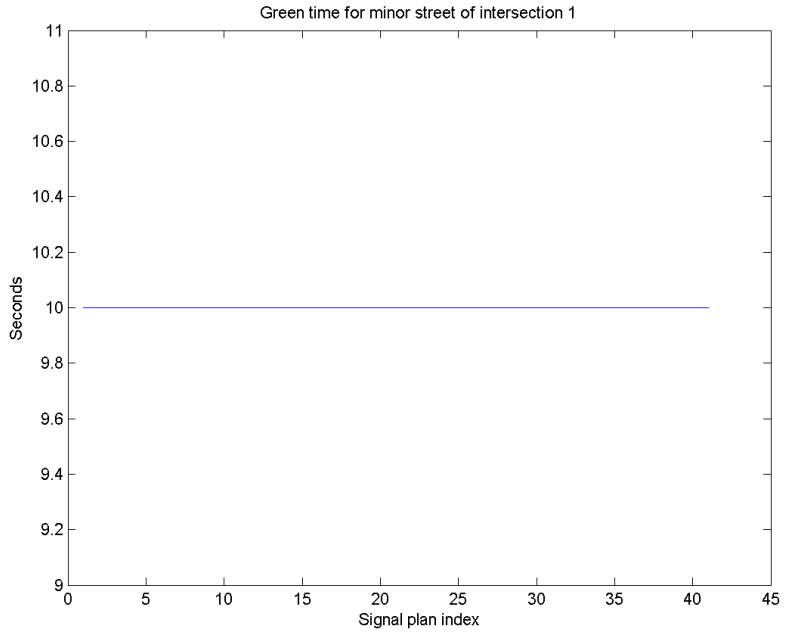

Figure 58. Green time for minor road of intersection 1 in platoon arrival case.

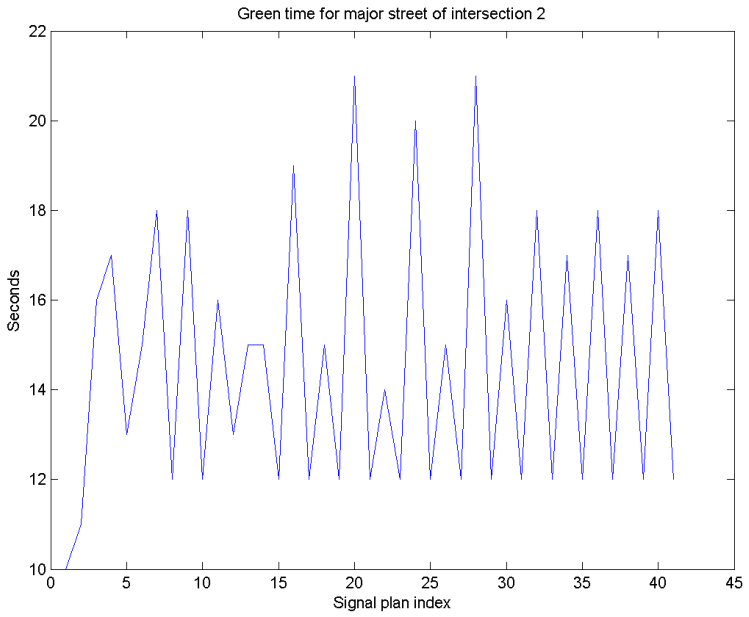

Figure 59. Green time for main arterial road of intersection 2 in platoon arrival case.

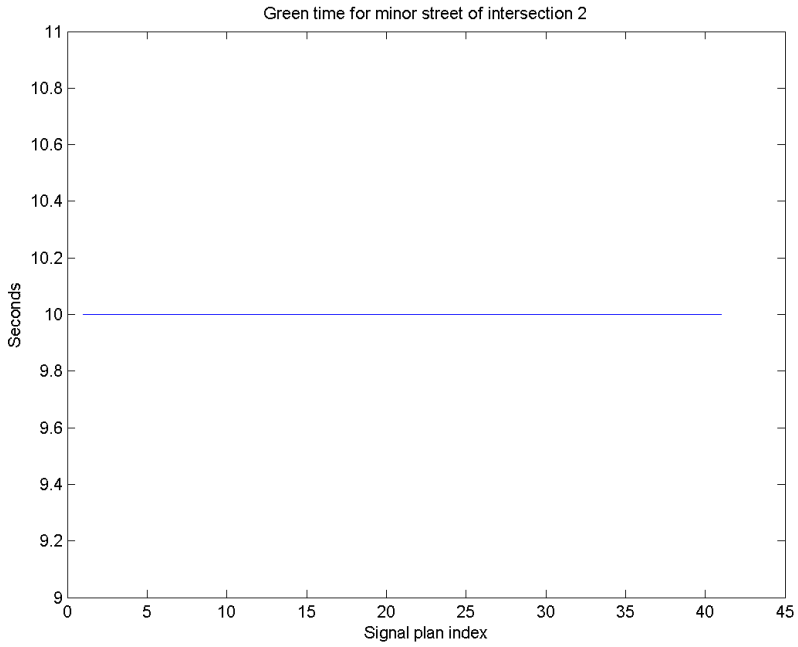

Figure 60. Green time for minor road of intersection 2 in platoon arrival case.

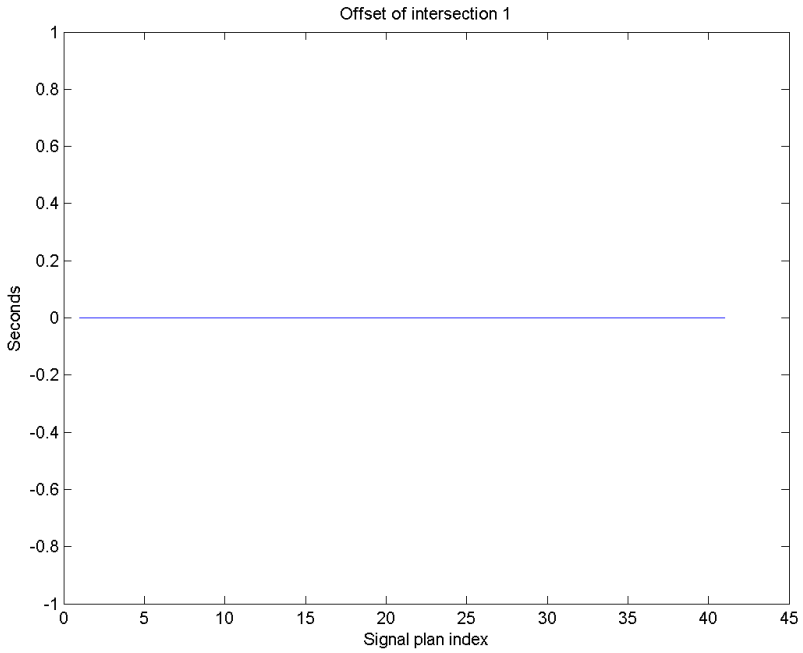

Figure 61. Offset of intersection 1 in platoon arrival case.

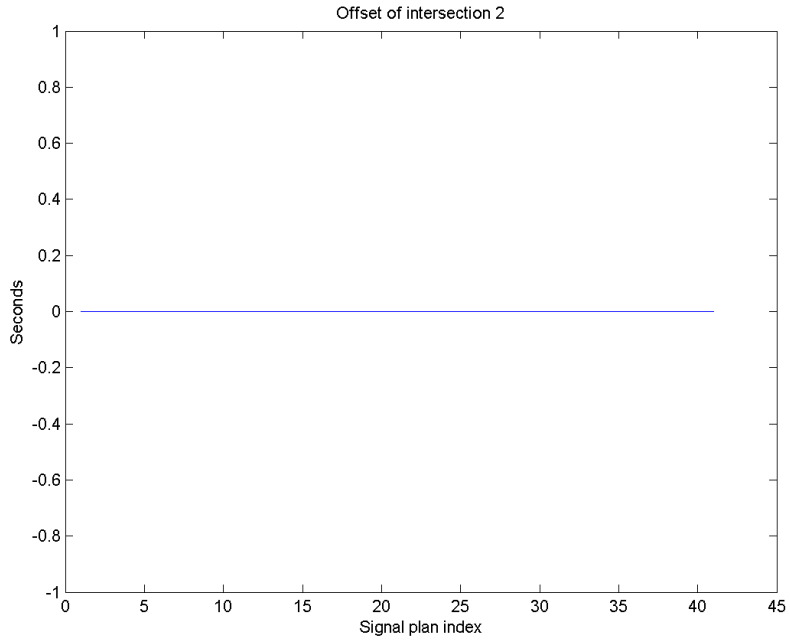

Figure 62. Offset of intersection 2 in platoon arrival case.

CHAPTER 5. CONCLUSIONS AND FUTURE WORK

Loop detectors are the most common detectors used in the United States. However, their maintenance and construction costs are their largest disadvantage. Also, loop detectors cannot be implemented to gather traffic data at every point. CVs can gather this traffic data; vehicles equipped with detectors travel along the road and provide traffic data in the spatial domain. Though this technology is promising, little research about it has been performed. Likewise, adaptive signal control has the potential to decrease delay time compared to pre-timed signals, but implementation of adaptive signal control in the United States is no more than 1 percent. Studies related to applying adaptive signal control with CVs are also few.

This study reviews adaptive signal control and past CV use. Most of the adaptive signal control logics/programs proposed in the past relied on loop detectors. A few of these adaptive signal control logics/programs, based on CV data, did not use the estimated queue as a variable to adjust the adaptive signal.

To achieve adaptive signal control logic for CVs, three methodologies were developed in this research project:

- A multi-class macroscopic model, M-CTM, was tested against S-CTM in coordination systems. The results imply that in a long arterial road or multi-class traffic, M-CTM should be used to find optimal offsets, rather than S-CTM. M-CTM could be integrated into adaptive signal control for the coordination mode.
- The algorithm to estimate the queue from CV data was proposed and verified with microscopic simulation, VISSIM. The results show that the estimation is accurate and consistent with queue data from VISSIM.
- An adaptive signal control logic with two modes depending on traffic condition was proposed. The results suggest that the algorithms can adapt between the two modes based on traffic condition.

Future work should extend and test the queue estimation algorithm with the arterial system. Another need is to improve the optimization module of adaptive signal control and to

test it on microscopic simulation such as VISSIM. Studying the effect of a penetration ratio on adaptive signal control should also be included in future work.

REFERENCES

[1] Work, Daniel B., O-P. Tossavainen, Sébastien Blandin, Alexandre M. Bayen, Toch Iwuchukwu, and Ken Tracton. "An Ensemble Kalman Filtering Approach to Highway Traffic Estimation Using GPS Enabled Mobile Devices." *47th IEEE Conference on Decision and Control*, 2008, pp. 5062–5068.

[2] Bayen, Alexandre M., Joe Butler, and Anthony David Patire. *Mobile Millennium Final Report*. California Center for Innovative Transportation, Institute of Transportation Studies, University of California, Berkeley, 2011.

[3] Pattara-Atikom, W., R. Peachavanish, and R. Luckana. "Estimating Road Traffic Congestion Using Cell Dwell Time with Simple Threshold and Fuzzy Logic Techniques." *Intelligent Transportation Systems Conference*, IEEE, 2007, pp. 956–961.

[4] Sohn, Keemin, and Daehyun Kim. "Dynamic Origin-Destination Flow Estimation Using Cellular Communication System." *IEEE Transactions on Vehicular Technology*, Vol. 57, No. 5, 2008, pp. 2703–2713.

[5] Meyer, Eric. "Analysis of Speed Data Derived from Cellular Probes." *15th World Congress on Intelligent Transport Systems and ITS America's 2008 Annual Meeting*, 2008.

[6] Amin, Saurabh, Steve Andrews, Saneesh Apte, Jed Arnold, Jeff Ban, Marika Benko, Re M. Bayen, et al. "Mobile Century Using GPS Mobile Phones as Traffic Sensors: A Field Experiment." 2008.

[7] Cheng, Peng, Zhijun Qiu, and Bin Ran. "Particle filter based traffic state estimation using cell phone network data." *Intelligent Transportation Systems Conference, 2006. ITSC'06. IEEE*, pp. 1047-1052. IEEE, 2006..

[8] Briesemeister, Linda, Lorenz Schafers, and Günter Hommel. "Disseminating Messages among Highly Mobile Hosts Based on Inter-vehicle Communication." *Proceedings of the IEEE Intelligent Vehicles Symposium*, 2000, pp. 522–527.

[9] Costa, Paolo, Davide Frey, Matteo Migliavacca, and Luca Mottola. "Towards Lightweight Information Dissemination in Inter-vehicular Networks." *Proceedings of the 3rd International Workshop on Vehicular Ad Hoc Networks*, 2006, pp. 20–29.

[10] Ott, Jörg, and Dirk Kutscher. "Drive-thru Internet: IEEE 802.11 b for" automobile" users." In *INFOCOM 2004. Twenty-third AnnualJoint Conference of the IEEE Computer and Communications Societies*, Vol. 1. 2004.

[11] Bychkovsky, Vladimir, Bret Hull, Allen Miu, Hari Balakrishnan, and Samuel Madden. "A Measurement Study of Vehicular Internet Access Using In Situ Wi-Fi Networks." *Proceedings*

of the 12th Annual International Conference on Mobile Computing and Networking, 2006, pp. 50–61.

[12] Research and Innovative Technology Administration, U.S. Department of Transportation. The Connected Vehicle Test Bed. http://www.its.dot.gov/testbed.htm, accessed Sept. 27, 2013.

[13] Hull, Bret, Vladimir Bychkovsky, Yang Zhang, Kevin Chen, Michel Goraczko, Allen Miu, Eugene Shih, Hari Balakrishnan, and Samuel Madden. "CarTel: A Distributed Mobile Sensor Computing System." *Proceedings of the 4th International Conference on Embedded Networked Sensor Systems*, 2006, pp. 125–138.

[14] U.S. Department of Transportation, Federal Highway Administration. Adaptive Signal Control. http://www.fhwa.dot.gov/everydaycounts/technology/adsc/ , accessed Sept. 27, 2013.

[15] Stevanovic, Aleksandar. *NCHRP Synthesis 403: Adaptive Traffic Control Systems: Domestic and Foreign State of Practice*. National Cooperative Highway Research Program, 2010.

[16] Skabardonis, Alexander, and Gabriel Gomes. *Effectiveness of Adaptive Traffic Control for Arterial Signal Management: Modeling Results.* California PATH Program, Institute of Transportation Studies, University of California at Berkeley, 2010.

[17] Martin, Peter T., and Stephen L.M. Hockaday. "SCOOT—An Update." *ITE Journal*, Vol. 65, No. 1, 1995.

[18] Sims, A. "SCAT: The Sydney Co-ordinated Adaptive Traffic System." *Symposium on Computer Control of Transport*, 1981, pp. 22–26.

[19] Gartner, Nathan H. "OPAC: A Demand-Responsive Strategy for Traffic Signal Control." *Transportation Research Record* 906, 1983.

[20] Head, K. Larry, Pitu B. Mirchandanai, and Steve Shelby. *The RHODES Prototype: A Description and Some Results*. University of Arizona, Tucson, Department of Systems and Industrial Engineering, 1998.

[21] Siromaskul, S., and M. Selinger. "InSync: The Next Generation of Adaptive Signal Systems." 2010.

[22] Cai, Chen, Yang Wang, and Glenn Geers. "Adaptive Traffic Signal Control Using Wireless Communications." *Transportation Research Board 91st Annual Meeting,* No. 12-2998, 2012.

[23] He, Qing, K. Larry Head, and Jun Ding. "PAMSCOD: Platoon-Based Arterial Multi-modal Signal Control with Online Data." *Transportation Research Part C: Emerging Technologies*, Vol. 20, No. 1, 2012, pp. 164–184.

[24] Webster, Fo Vo. *Traffic Signal Settings*. No. 39, 1958.

[25] Daganzo, Carlos F. "The Cell Transmission Model: A Dynamic Representation of Highway Traffic Consistent with the Hydrodynamic Theory." *Transportation Research Part B: Methodological,* Vol. 28, No. 4, 1994, pp. 269–287.

[26] Daganzo, Carlos F. "The Cell Transmission Model, Part II: Network Traffic." *Transportation Research Part B: Methodological,* Vol. 29, No. 2, 1995, pp. 79–93.

[27] Lo, Hong K., Elbert Chang, and Yiu Cho Chan. "Dynamic Network Traffic Control." *Transportation Research Part A: Policy and Practice,* Vol. 35, No. 8, 2001, pp. 721–744.

[28] Comert, Gurcan, and Mecit Cetin. "Queue Length Estimation from Probe Vehicle Location and the Impacts of Sample Size." *European Journal of Operational Research,* Vol. 197, No. 1, 2009, pp. 196–202.

[29] Comert, Gurcan, and Mecit Cetin. "Analytical Evaluation of the Error in Queue Length Estimation at Traffic Signals from Probe Vehicle Data." *IEEE Transactions on Intelligent Transportation Systems,* Vol. 12, No. 2, 2011, pp. 563–573.

[30] Comert, Gurcan. "Effect of stop line detection in queue length estimation at traffic signals from probe vehicles data." *European Journal of Operational Research* Vol. 226, No. 1, 2013, pp. 67-76..

[31] Comert, Gurcan. "Simple Analytical Models for Estimating the Queue Lengths from Probe Vehicles at Traffic Signals." *Transportation Research Part B: Methodological,* Vol. 55, 2013, pp. 59–74.

[32] Cheng, Yang, Xiao Qin, Jing Jin, and Bin Ran. "An Exploratory Shockwave Approach for Signalized Intersection Performance Measurements Using Probe Trajectories." *Transportation Research Board 89th Annual Meeting,* No. 10-1617, 2010.

[33] Izadpanah, Pedram, Bruce Hellinga, and Liping Fu. "Automatic Traffic Shockwave Identification Using Vehicles' Trajectories." *Proceedings of the 88th Annual Meeting of the Transportation Research Board* (CD-ROM), 2009.

[34] Hao, Peng, and Zhanbo Sun. "Real Time Queue Length Estimation for Signalized Intersections Using Travel Times from Mobile Sensors." *Transportation Research Part C: Emerging Technologies,* Vol. 19, No. 6, 2011, pp. 1133–1156.

[35] Sun, Zhanbo, and Xuegang Jeff Ban. "Vehicle Trajectory Reconstruction for Signalized Intersections Using Mobile Traffic Sensors." *Transportation Research Board 91st Annual Meeting,* No. 12-4279, 2012.

[36] Abishek, C., Mukul Kumar, and P. Kumar. “City Traffic Congestion Control in Indian Scenario Using Wireless Sensors Network.” *2009 Fifth IEEE Conference on Wireless Communication and Sensor Networks (WCSN)*, 2009, pp. 1–6.

[37] Gradinescu, Victor, Cristian Gorgorin, Raluca Diaconescu, Valentin Cristea, and Liviu Iftode. “Adaptive Traffic Lights Using Car-to-Car Communication.” *IEEE 65th Vehicular Technology Conference*, VTC2007-Spring, 2007, pp. 21–25.

[38] Tuerprasert, Kamonthep, and Chaodit Aswakul. “Multiclass Cell Transmission Model for Heterogeneous Mobility in General Topology of Road Network.” *Journal of Intelligent Transportation Systems*, Vol. 14, No. 2, 2010, pp. 68–82.

[39] Halati, Abolhassan, Henry Lieu, and Susan Walker. “CORSIM-Corridor Traffic Simulation Model.” *Traffic Congestion and Traffic Safety in the 21st Century: Challenges, Innovations, and Opportunities*, 1997.

[40] Chui, Charles K., ed. *An introduction to wavelets*. Vol. 1. Academic press, 1992.

[41] Akansu, Ali N., and Paul R. Haddad. *Multiresolution signal decomposition: transforms, subbands, and wavelets*. Academic Press, 2000.